

MSc Thesis Report

Simulating 3D Sand Wave Recovery
After Pre-sweeping by Delft3D FM

TAM, Tsz Fung (Zeta)

MSc Thesis Report

Simulating 3D Sand Wave Recovery After Pre-sweeping by Delft3D FM

by

TAM, Tsz Fung (Zeta)

to obtain the degree of Master of Science in Civil Engineering (Track: Hydraulic Engineering)

at the Delft University of Technology,

to be defended publicly on Thursday August 31, 2023 at 3:00 PM.

Student number:	5448182
Project duration:	November, 2022 – August, 2023
Committee Members:	Prof. Dr. Ir. Ad Reniers TU Delft
	Dr. Ir. Bram van Prooijen TU Delft
	Dr. Ir. Arjen Luijendijk TU Delft, Deltares
	Ir. Pauline Overes UTwente, Deltares

Cover: Generated by DALL-E in December 2022 and modified by Zeta
 Tam

Style: TU Delft Report Style, with modifications by Daan Zwaneveld

An electronic version of this thesis is available at <http://repository.tudelft.nl/>.

Preface

This master's thesis marks the end of my two-year student life at Delft University of Technology and finishes my master's degree in Civil Engineering with a track in hydraulic engineering. Time flies. I still remember the moment when I felt confused and was struggling with being a civil engineer in Hong Kong three years ago. Reaching the fifth year of my career, I felt stuck in my career development. Then, I decided to take a pause and specialise in hydraulics to follow my passion. I finally selected TU Delft because of its curriculum and its reputation and I did not regret the choices I made. Throughout these two years, I had continuously broken my limits, created lots of ideas, obtained precious knowledge and experiences from all the experts and professors from TU Delft and Deltares and experienced an untypical student life in Svalbard, Norway. These experiences made me realise that I can go much further and encounter more.

This research was in collaboration with Deltares and I would like to thank Arjen Luijendijk and Pauline Overes for their continuous and inspirational advice. They always unselfishly share their knowledge and express their ideas on sand waves and morphological modelling, Especially Arjen, he always has fantastic ideas and encourages me to think and achieve more. I also appreciate Pauline devoting her time to review my thesis report again and again.

I would also like to thank Ad Reniers and Bram van Prooijen for being a part of my committee. Their critical views on the thesis made me recognise the significance and the value of the works that I have done. To Ad, I am so grateful to have you as a reliable chairperson solving issues together.

In addition, I would like to thank all the friends which I met in Delft and Svalbard. You all added colour to my life and I am glad we had remarkable moments together.

Last but not least, I would like to express my gratitude to my family for letting me explore the world for two years without any worries.

To end this preface, I would like to share a motto to remind myself in the future and encourage the readers of this thesis: Keep breaking your limits and see how far you can go in your limited life.

TAM, Tsz Fung (Zeta)
Delft, August 2023

Summary

The European Union strives for rapid development of offshore wind energy due to environmental and geopolitical issues. The offshore wind energy in Europe is mainly clustered in the North Sea due to its favourable metocean condition and the proximity to neighbouring countries. However, there are various morphological features covering the seabed in the North Sea, such as sand waves. Sand waves are one of the large-scale morphological features under the sea and are problematic to marine transport and offshore infrastructure. For example, the migration of sand waves causes exposure and failure of submarine cables. Pre-sweeping is usually involved in submarine utility installation in order to facilitate the installation work and reduce the impact of sand waves. This measure is a temporary solution and sand waves commonly recover after years. Given that the recovery process is well-investigated, a better dredging planning can be achieved. However, this process is currently not well-studied and the existing models of estimating sand wave recovery have their limitations, such as low applicability due to their empirical nature or limited dimension of the models. Thus, this master's thesis aims to gain more understanding of sand wave recovery from a pre-sweeping case and the capability of Delft3D FM in modelling this phenomenon through a case study.

A location in the Southern North Sea is chosen and studied. According to available information, pre-sweeping was carried out in the study area in 2018. From the bathymetry measurement data in 2016 and 2021 available on EMODnet, several phenomena were identified, including sand wave recovery, sand wave migration and interaction between dredged and non-dredged areas, such as an elevation drop in the non-dredged area.

Subsequently, a 3D numerical model was built in Delft3D FM to study the sand wave recovery in the study area and examine its modelling performance. This model is the first 3D numerical model specifically for simulating sand wave recovery after pre-sweeping with sufficiently fine grid sizes and the hydrodynamic performance was validated by the DCSM. With the aid of DelftBlue, an HPC cluster at Delft University of Technology, and MORFACs, which is a factor for morphological upscaling, the computational effort for this heavy simulation can be significantly reduced.

It is found that the sand wave recovery process is a local redistribution of sediment and the transverse slope effect and direct filling by flow are two reasons causing sediment infilling into the dredged trench. The transverse slope effect induces an additional downslope bed load transport which could lead to a significant infilling amount. The evolution of the seabed level was also analysed and two stages in the sand wave recovery are identified. The first stage refers to the initial morphological adjustment of the dredged profile adapting the forcing and the second stage refers to the growth of a morphological feature developed during the adaption period. In the meantime, through a sensitivity analysis, it is found that MORFAC, varying from 1 to 360 would not affect the topographic evolution but the simulation results contain a slight difference in the final seabed level among different MORFACs.

This pioneering research provides viewpoints of both physical processes and numerical modelling perspectives on sand wave recovery. This study not only provides a physical explanation of how tidal flow drives the recovery and how the morphology develops during the recovery, but also reveals the accomplishment of Delft3D FM in modelling this phenomenon with the upscaling techniques. Although the precise estimation of the recovery duration by Delft3D FM remains challenging, the findings in this study deliver implications for the further exploration of this subject, for instance, the calibration of the user-defined parameter α_{bn} , the impact of storms and the influence of the trench configuration.

Contents

Preface	i
Summary	ii
1 Introduction	1
2 Research Objectives	4
2.1 The Main Objective	4
2.2 Research Questions	4
2.3 Scope	5
3 Literature Review	6
3.1 A Subsea Morphological Feature - Sand Waves	6
3.1.1 Sand Wave and its Characteristics	6
3.1.2 Sand Waves and its Dynamics	6
3.1.3 Linear Stability Analysis of Sand Waves Growth	9
3.2 Sand Wave Dredging and Recovery	10
3.2.1 Observations	10
3.2.2 Modelling sand wave recovery	13
3.3 A Process-based Model - Delft3D FM	14
3.3.1 Hydrodynamic Modelling	15
3.3.2 Morphodynamic Modelling	16
4 Case Study - NEMO Link	19
4.1 Background Information	19
4.2 Hydrodynamic Condition at the AOI	21
4.3 Sand Wave Characteristics	23
4.3.1 Analysis Methods	23
4.3.2 Sand Wave Height	25
4.3.3 Sand Wave Migration	25
4.3.4 Recovered Sand Wave Shape	26
4.4 Sediment Budget	28
4.4.1 Analysis Methods	28
4.4.2 Results	29
4.5 Summary	31
5 Numerical Modelling	32
5.1 Model Setting	32
5.1.1 Computational Grid and Vertical Discretisation	32
5.1.2 Bathymetry	33
5.1.3 Boundary Conditions	34
5.1.4 Sediment Parameters	35
5.1.5 Sediment Transport Formulation	35
5.2 Hydrodynamic Performance of the Model	37
5.3 Simulation Scenarios	37
5.4 Simulation Results	38
5.4.1 Pre-dredging Case	38
5.4.2 Post-dredging Case	39
5.5 Discussion of the Results	40
5.5.1 Hydrodynamic and Morphodynamic Perspective of sand wave recovery	40
5.5.2 Staging in Sand Wave Recovery	44

5.5.3	Outcome of Various MORFAC	45
6	Discussion	48
6.1	Sand Wave Recovery Mechanisms	48
6.2	Staging of Sand Wave Recovery	48
6.3	Capability of Delft3D FM in Modelling Sand Wave Recovery	49
6.4	Upscaling with MORFAC and HPC	50
6.5	Impact of Storm	50
7	Conclusion	51
7.1	Answers to the Research Questions	51
7.2	Limitations of This Thesis	52
7.3	Recommendations	52
	References	54
A	Sensitivity Analysis of Various Parameters	56
A.1	Use of Different Van Rijn Formulations	56
A.1.1	Van Rijn (1993 & 2007) Formulations	56
A.1.2	Results Comparison	57
A.2	User-defined Tuning Parameter (α_{bs})	58
A.3	Median Grain Size	59

1

Introduction

The European Union is ambitious to promote renewable energy in view of environmental and geopolitical issues and several strategies were proposed. For instance, the 2050 long-term strategy was proposed to strive for a carbon-neutral continent by 2050, which is in line with the EU's commitment under the Paris Agreement [9], and the "REPowerEU" plan was also implemented to enhance the energy dependence of the EU and secure the energy supply [10]. To achieve these objectives, an expansion of offshore wind energy is one of the measures.

The offshore wind energy development in Europe is tremendous and rapid. The cumulative installed capacity of offshore wind energy had increased sevenfold from 3GW in 2010 to 22GW in 2019 among all European countries, including the UK [15]. Among all sea basins in Europe, the majority of offshore wind turbines were installed in the North Sea and it occupied 77% of the cumulative installed capacity in 2019 [15]. It is shown that the North Sea is a significant area for offshore wind energy development. The offshore wind turbines in Europe are mainly clustered in the North Sea because it is an ideal area providing relatively shallow water and a favourable climate. This favours the construction of offshore wind farms and provides a reliable wind source.

In the meantime, there are different seabed bedforms covering the North Sea. Sand waves as shown in Figure 1.2, which are one of the large-scale morphological features with a typical wave height of metres and wavelength of hundreds of metres, cover a large extent of the area in the Southern North Sea. Compared with the location of offshore wind farms location, including those planned and constructed, some of the offshore wind farms are located in these sand wave fields, as shown in Figure 1.1, because of the proximity to neighbouring countries.

Sand waves are a nuisance to marine transport, offshore structures and offshore utilities during both the operation and construction stages. For example, the migration of sand waves causes exposure of submarine cable, and thus, a failure of the cable [28]. On the other hand, the migration of sand waves can fill up an open trench for submarine cable installation. To deal with the issues associated with sand waves, these morphological features are commonly dredged by pre-sweeping. Pre-sweeping is a construction procedure to facilitate submarine utility installation and reduce the impact of sand waves on the utility by dredging existing sand waves.

Sand wave recovery usually occurs after dredging and examples can be found in the North Sea or in Japan [20, 6, 23] but sand wave recovery is an underexplored topic. Existing publications focused yearly development of sand wave recovery after large-scale dredging and provided limited information on sand wave recovery after pre-sweeping in submarine cable installation. Observations from a UK offshore windfarm project showed two distinctive phases of sand wave recovery and an interaction between the dredged and non-dredged area occurred in the vicinity after dredging [24] but there is no solid explanation of physical processes involved or the spatial and temporal development of sand wave recovery. More research is necessary to investigate the sand wave recovery processes.

Considering the whole scale of a construction project and assuming that the regeneration of sand

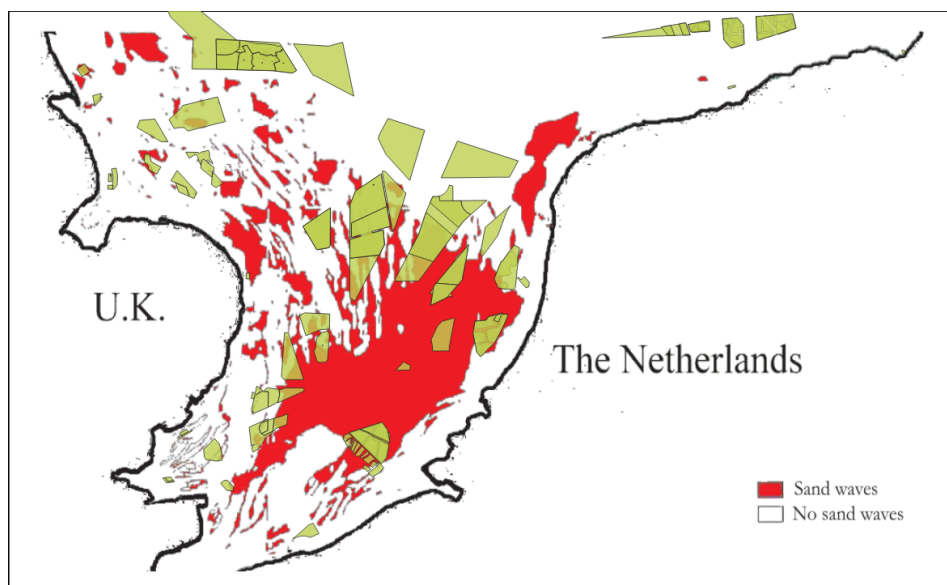


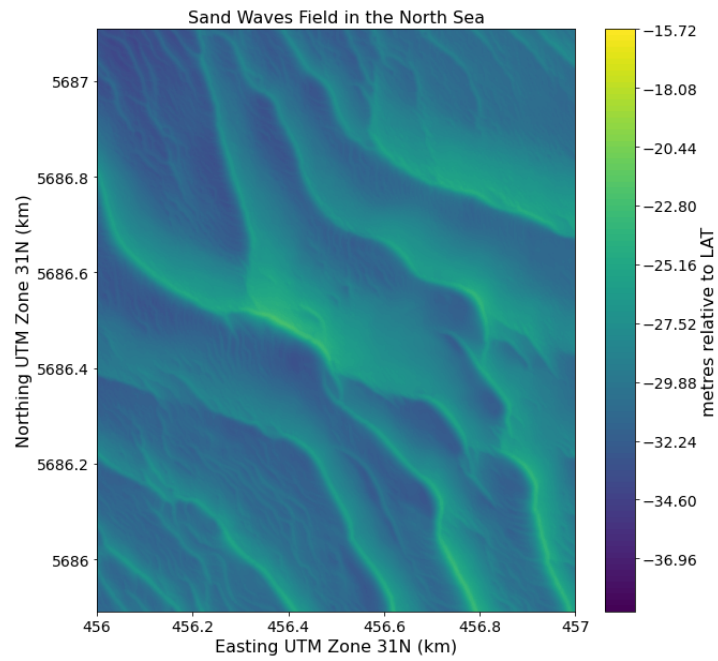
Figure 1.1: A Composite Image of Offshore Wind Farms Areas [14] and Sand Waves Coverage in the Southern North Sea [29]
(Green shaded areas show the extent of offshore wind farms)

waves at different locations in a project area is known, not only how high the sand wave is known at a particular time, but also at the time when it regenerates, the resources for dredging, such as equipment and vessels, during both construction and maintenance can be optimised, and thus, costs, time and carbon footprint can be reduced. Predicting the regeneration of sand waves can enable more effective and efficient planning of dredging works and the design of offshore constructions. However, reviewing the previous studies, the models estimating sand wave recovery have lower applicability due to their empirical nature and the limitation of a 2DV setting, which cannot take the interaction between non-dredged and dredged areas into account. Delft3D, a process-based model, is increasingly involved in modelling sand wave dynamics and recovery. It could be a potential tool to break these limitations and help understand the recovery mechanisms and the recovery duration.

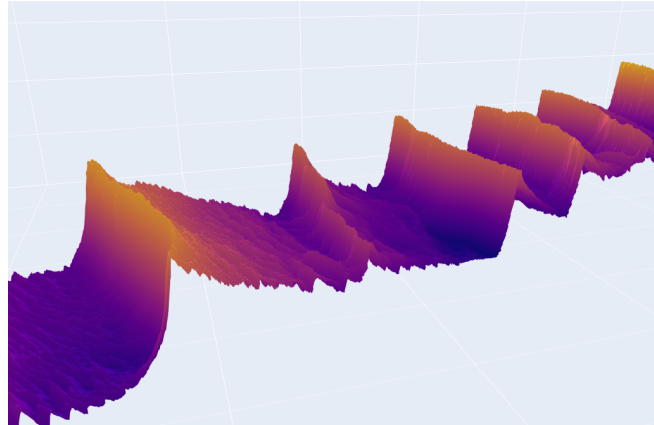
Therefore, this master's thesis aims to gain an understanding of sand wave recovery after pre-sweeping and the capability of Delft3D Flexible Mesh (FM) in simulating the recovery process spatially and temporally. Through a desktop study and morphodynamic modelling carried out in this thesis, more information related to sand wave recovery mechanisms and Delft3D FM capability is revealed. In this thesis, a supercomputer, namely DelftBlue, at the Delft University of Technology was utilised to reduce the computational effort.

This report consists of 7 different chapters, including this Chapter 1: Introduction. Chapters 2 and 3 detail the research objectives of this thesis and the current research development on sand wave recovery, and are followed by Chapters 4 and 5 which explain the methodology and findings from a case study and numerical modelling. Finally, this thesis is summarised and concluded by a discussion in Chapter 6 and a conclusion in Chapter 7.

This master's thesis is in collaboration with Deltares, which is based in Delft, the Netherlands.



(a) An Example of Sand Waves Field in the North Sea
(The yellowish-green lines indicate the crests of sand waves)



(b) A 3D Impression of Sand Waves
(Vertical scale is exaggerated for illustration)

Figure 1.2: Impression of Sand Waves in the North Sea

2

Research Objectives

2.1. The Main Objective

The main objective of this study is as follows:

What are the key sand wave recovery processes after pre-sweeping and what is Delft3D FM capability of simulating them in a 3D setting?

This thesis aims to gain an understanding of the sand wave recovery process after pre-sweeping, such as how tidal current flows over a dredged trench and how sediment is transported into the trench, and find out the capability of Delft3D FM in modelling such a process spatially and temporally to see whether Delft3D FM has potential to predict sand wave recovery development and what challenges there are in modelling the process.

2.2. Research Questions

The main objective involves two aspects: First, the sand wave recovery process is focused:

1. How does a sand wave recover and what are the key processes behind sand wave recovery process?

The first question focuses on the mechanisms behind sand wave recovery. It is intriguing to know what processes are involved during the complete recovery process. To answer this question, a case study was simulated by Delft3D FM. The use of a numerical model provides detailed information on the evolution of sand waves and the hydrodynamic environment in the area. As such, the hydrodynamics and morphodynamics of sand wave recovery are revealed.

Second, this thesis also endeavours on delivering the capability of Delft3D FM in modelling sand wave recovery spatially and temporally. Delft3D FM was used because it was demonstrated that Delft3D FM was able to model sand wave dynamics with increased modelling efficiency, parallel computing ability and aid of unstructured grids [31]:

2. To what extent is Delft3D FM able to simulate the key sand wave recovery processes after pre-sweeping in a 3D setting?
3. To what level can Delft3D FM estimate the timescale of sand waves regeneration?

The knowledge of sand wave recovery is limited. The existing mathematical model also lacks the full picture of physical processes and measurement data can only provide intermittent information. If Delft3D FM is capable of simulating sand wave recovery processes, it can provide us a detailed spatial and temporal topography development of sand waves. In addition, 2DV models were adopted in past

publications because they focused on sand waves growth and migration, in which sand waves were likely uniform in the transverse direction, and the vertical circulation induced by an interaction between tidal current and bedforms was concerned. However, publications showed an interaction between dredged and non-dredged areas during sand wave recovery, which cannot be modelled in a 2DV model. Thus, this thesis aims to develop a 3D model showing sand wave recovery processes.

To achieve this, a comparison between model results and other information from existing literature and case study was made to see whether Delft3D FM is able to provide similar outcomes shown in the literature and the case study.

Finally, this thesis attempts to extend our knowledge of upscaling techniques in 3D morphodynamic modelling:

4. What is the order of magnitude of critical MORFAC in modelling 3D morphodynamics of pre-sweeping?

MORFAC is one of the upscaling techniques to increase model efficiency. If the MORFAC is too high, the linear assumption is no longer valid leading to an unrealistic morphological change [32]. Thus, MORFAC should be chosen carefully to allow faster computation with a realistic result. As experience in 3D morphodynamic modelling is limited and an appropriate value of MORFAC is case-specific, this research question aims to provide an idea for choosing MORFAC for modelling sand wave recovery in a 3D model through a sensitivity analysis.

2.3. Scope

This thesis focuses on sand wave recovery after pre-sweeping before cable installation. However, in the literature study, past publication related to sand wave recovery after other dredging activities was also considered because it is believed that they might provide insight into the sand wave recovery process in a certain extent.

Spatial variability of soil properties is not a focus of this thesis. It is acknowledged that the mobility of sediment affects erosion and accretion but information related to spatial variability of sediment properties can be limited unless extensive geotechnical investigation has been carried out. In addition, this thesis aims to provide more understanding of sand wave recovery due to hydrodynamic processes so the influence of soil properties was not considered.

On the other hand, sediment input is assumed sufficient for sand wave regeneration. In the past publication, it was explained that sediment availability is one of the factors affecting sand wave regeneration [23]. Since a case study with sand wave regeneration was studied and modelled, this implies that there is no deficiency in sediment input.

The location of morphodynamic modelling is limited to an area in the North Sea, which is introduced in Chapter 4, because of two reasons. First, publicly accessible measurement data is available online, which means that data for model calibration or validation is available. Second, the metocean condition in the North Sea is less complicated, compared with other ocean basins in Europe.

3

Literature Review

3.1. A Subsea Morphological Feature - Sand Waves

3.1.1. Sand Wave and its Characteristics

In the North Sea, the subsea topography is covered by rhythmic bed features, including ripples, megaripples, sand waves and sand banks. These features are characterised by their own wave height, wavelength and mobility and developed by the interaction among hydrodynamics, sediment transport and morphology. The typical length scales of these features are tabulated in Table 3.1 [28].

Morphological Feature	Wave Amplitude	Wavelength
Ripples	O(0.01m)	O(0.01m)
Megaripples	O(0.1m)	O(10m)
Sand Waves	O(5m)	O(500m)
Sand Bank	O(10m)	O(5000m)

Table 3.1: Typical Characteristics of Morphological Features

In this thesis, only sand waves in the North Sea are focused on. The wavelength of sand waves is in the order of hundreds metres and its wave height is in order of metres in the North Sea. [27]. In fact, sand waves can reach more than 10m in wave height, such as sand waves in Taiwan Straits [2].

A sand wave is usually not a single morphological feature appeared in an area and usually accompanies by other morphological features. For example, sand waves with superimposed megaripples were observed in a region of the North Sea southwest of IJmuiden [27] and sand waves overlying a sand-bank were also observed in the Race Bank Wind Farm project in the UK [25]. These features influence each other.

Apart from the distinctive dimension of sand waves, sand waves can also be characterised by their shapes. Van Veen [39] categorised sand waves (in the order of 10m height and 200m wavelength) into two main classes: symmetrical or trochoidal, and asymmetrical or progressive. Under the class of asymmetrical wave, asymmetrical and “catback” form as shown in Figure 3.1 can be found.

The orientation of sand wave crests is usually perpendicular to the major axis of tidal ellipse based on the observation on field data [18].

3.1.2. Sand Waves and its Dynamics

Sand Waves Growth and Migration

As perturbation on the seabed exists, the tidal current interacts with the perturbation.

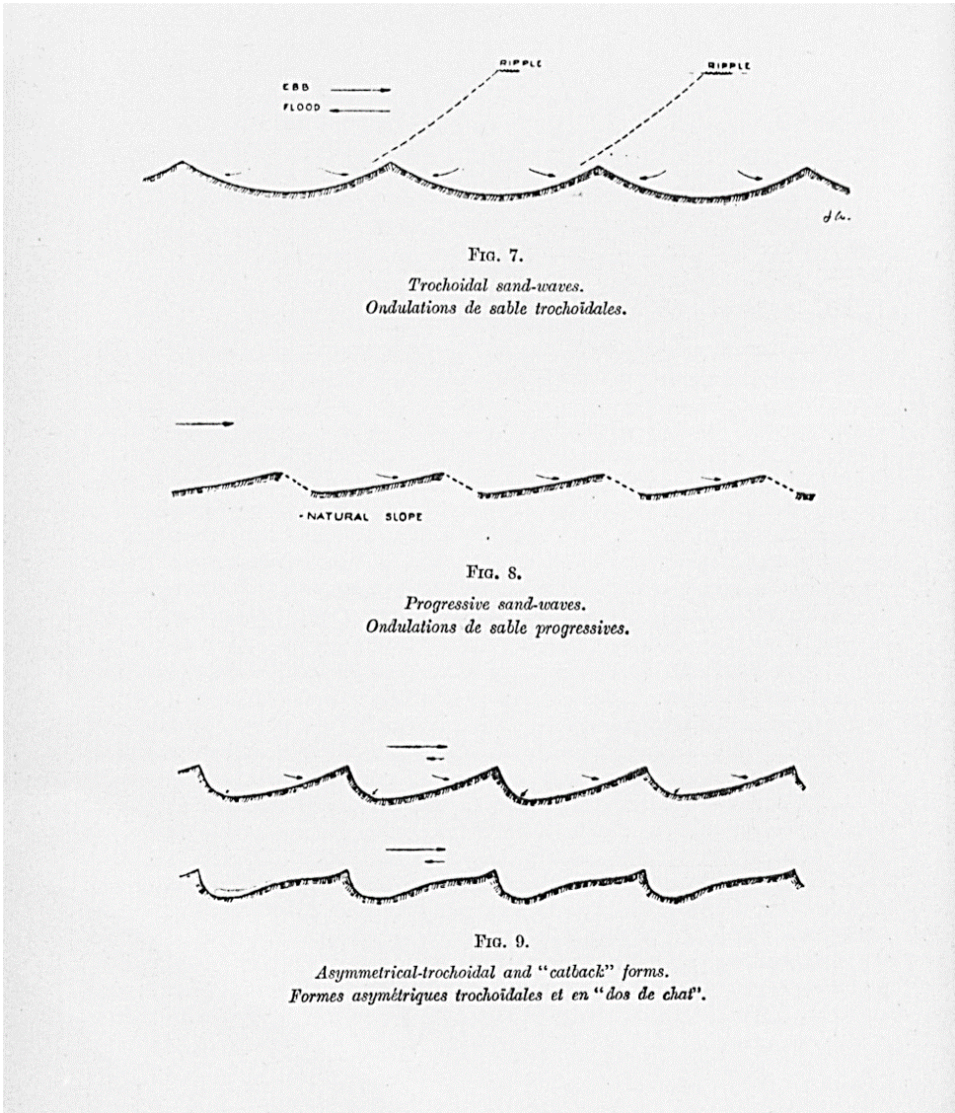


Figure 3.1: Different Shapes of Sand Waves (Reproduced from Van Veen [39])

As tidal current flows over existing bedforms, the current accelerates as the flow depth decreases at the stoss side of bedform and decelerates as the flow depth increases at the leeside of bedform. As a result, there is a net current causing downstream sediment transport, as shown in Figure 3.2a. During a symmetrical tide, flood and ebb tides flow in different directions and, as a result, the tidal forcing accumulates sediment at existing bedform and causes development of bedform as shown on Figure 3.2b. A near-bed circulation is formed due to interaction between tidal forcing and bedforms as shown in Figure 3.3. On the other hand, when this tidal current circulation becomes asymmetric, there is a net sediment transport to one direction, such as due to higher tide components or residual current, which implies the migration of bedform [29, 3].

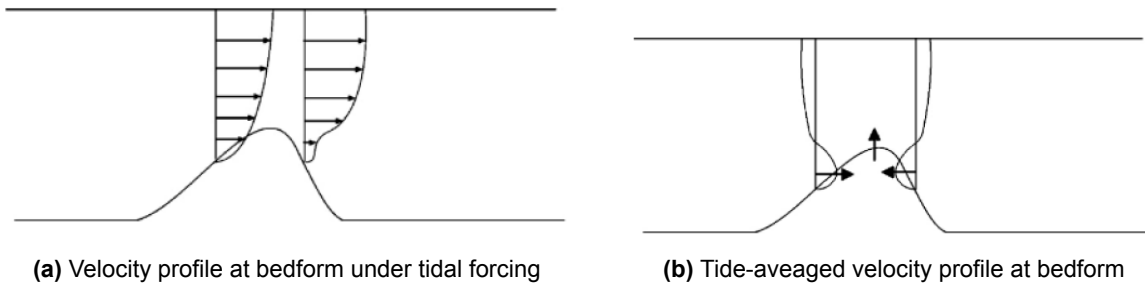


Figure 3.2: Velocity profile at bedform due to tidal forcing (Reproduced from Tonnon et al. [36])

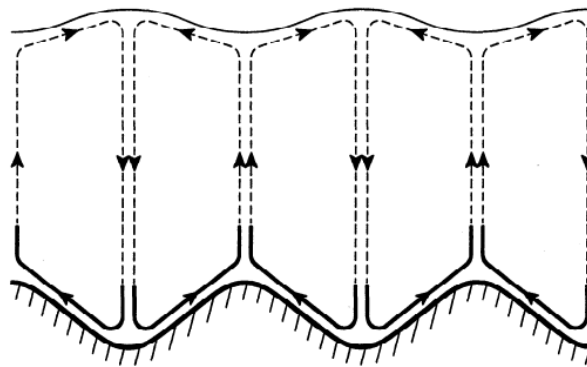


Figure 3.3: Near-bed circulation due to interaction of tide and bedform (Reproduced from Hulscher [18])

According to the linear stability analysis developed by Hulscher [18], a range of sand waves with different wave length is possible due to the near-bed interaction, but there is a unique fastest growth mode. The fastest growth mode of a bed feature refers to the particular or preferred form, such as a particular wave length or orientation, of a bed feature. Such particular form commonly appears in a location and is obviously observed.

The mode of sediment transport can affect the growth or the shape of sand waves. McCave [27] analysed the field observation data in the front of the Dutch Coast. It was observed that the sand wave height decreased as it went northward and it was explained that as it went northward, the grain size decreased, and thus, the dominant sediment transport mode shifted to suspended load transport, which was unfavourable to sand wave growth. Later, Borsje et al. [5] studied the role of suspended load transport by using process-based morphological model, Delft3D, and field data and it is concluded that bed load transport causes sand waves growth and suspended load transport dampened the growth of long sand waves. As a result, if the dominant sediment transport mode is suspended load transport, no sand wave is observed due to the net dampening effect of suspended load transport.

From classification given by Fredsøe and Deigaard [16], the dominant sediment transport mode can

be determined by Rouse Number. Rouse number is the ratio between the settling velocity of sediment and upward motion due to turbulence and is expressed as follows:

$$R = \frac{w_s}{\kappa u_*} \quad (3.1)$$

where w_s is settling velocity of sediment, κ is Von Karman constant and u_* is friction velocity.

According to Fredsøe and Deigaard [16], if the Rouse number is smaller than 1.2, the transport regime is classified as suspended load transport. If it is larger than 2.5, the transport regime is classified as bed load transport. In between these two values, incipient suspended load transport is classified. Borsje et al. [5] found that the lower limit of sand wave occurrence was at $R = 1.9$ based on field data from the southern North Sea or $R = 2.0$ based on Delft3D simulations.

On the other hand, the slope of bedform acts an important role in sand waves growth. An experiment carried out by Smart [34] showed an obvious increase in sediment transport rate as the gradient of bed slope increased. Van Rijn [38] believed that the bed slope might affect sediment transport in three different aspects, including local near-bed flow velocity, threshold conditions and sediment transport rate once the sediment is in motion. Since the gravitational effect leads to higher difficulty for sediment moving upslope than downslope, the sediment is transported from the crest to the trough under a tide-averaged flow and such a transport causes dampening of sand waves.

To sum up, sand wave dynamics are mainly due to the interaction between tidal forcing and bedforms. Sand waves grow due to a tidal current circulation and migrate due to an asymmetrical tidal current circulation. On the other hand, the gradient of bedforms prohibits the growth of sand waves and facilitates dampening. In the meantime, the grain size determines dominant sediment transport modes, and thus, dampening and growth of sand waves. As a result, the interaction between sand waves growth and dampening process causes the dominance of the fastest growth mode.

3.1.3. Linear Stability Analysis of Sand Waves Growth

A three-dimensional model developed by Hulscher [18] describes the growth of sand wave and other features, which are formed due to interaction between tidal current and bedform with dampening by slope correction effect. In the case of sand waves, the Coriolis effect in sand wave is limited due to its dimension and the sand wave crests are oriented almost perpendicular to the tidal motion.

Hulscher developed a coupled model based on three-dimensional shallow water equations. The choice of shallow water equations is based on the fact that tidal wave is considered as a long wave in a coastal water. The coupled model consists of a flow model and a sediment transport model.

The flow model is the shallow water equations shown as follows:

$$\frac{\partial u}{\partial t} + u \frac{\partial u}{\partial x} + v \frac{\partial u}{\partial y} + w \frac{\partial u}{\partial z} - fv = -g \frac{\partial \zeta}{\partial x} + \frac{\partial}{\partial z} (A_v \frac{\partial u}{\partial z}) \quad (3.2)$$

$$\frac{\partial v}{\partial t} + u \frac{\partial v}{\partial x} + v \frac{\partial v}{\partial y} + w \frac{\partial v}{\partial z} + fu = -g \frac{\partial \zeta}{\partial y} + \frac{\partial}{\partial z} (A_v \frac{\partial v}{\partial z}) \quad (3.3)$$

$$\frac{\partial u}{\partial x} + \frac{\partial v}{\partial y} + \frac{\partial w}{\partial z} = 0 \quad (3.4)$$

where u , v and w are the velocity components in the x-, y- and z-directions, ζ is water elevation above a reference level, f is the Coriolis parameter, g is the gravitational acceleration and A_v is vertical viscosity.

On the other hand, the sediment transport model consists of the following general formula:

$$S_b = \alpha |\tau|^b \left\{ \frac{\tau}{|\tau|} - \lambda \nabla h \right\} \quad (3.5)$$

where S_b is the sediment transport vector, α is the bed load transport proportionality parameter, λ is the bed-slope correction term and τ denotes the shear stress at the bottom:

$$\tau = A_v \left(\frac{\partial u}{\partial z}, \frac{\partial v}{\partial z} \right) \Big|_{z=\text{bottom}} \quad (3.6)$$

Finally, the sediment transport model is coupled with the sediment balance equation and the change in seabed level can be calculated:

$$\frac{\partial h}{\partial t} + \nabla S_b = 0 \quad (3.7)$$

Further, Hulscher [18] expressed the equations in a dimensionless form and there are two significant dimensionless parameters, vertical Stokes Number (E_v) and dimensionless resistance parameter (\hat{S}). The vertical Stokes Number describes the influence of the vertical viscosity effect on the tidal motion in the water column and the dimensionless resistance parameter quantifies the amount of resistance at the bottom. Different combinations of these two parameters result in different characteristics of the fastest growing mode, including its wave number, direction and growth rate. Thus, different bedforms, such as sand waves or sand banks, are determined.

3.2. Sand Wave Dredging and Recovery

3.2.1. Observations

Sand wave is problematic to submarine cables or pipelines and also impacts their construction because, as it migrates, the buried cables or pipelines would be exposed and damaged or the trench could also be filled during the construction.

For instance, Morelissen [28] schematised how migration of sand waves could lead to pipeline exposure as shown in Figure 3.4 and also stated that exposed submarine pipelines may result in pipeline failure or rupture due to lost of support or may obstruct other offshore activities, such as fishing and anchoring.



Figure 3.4: Illustration of Pipe Exposure due to Sand Waves Migration: Dotted line represents sand wave profile and solid line represents pipe alignment [28]

Pre-sweeping is a construction procedure commonly involved in submarine cable installation to remove existing sand waves. The purpose of this procedure is to remove unfavourable steep slopes caused by sand waves for operation of cable installation equipment and reduce nuisance to installed submarine cable in operation phase. Pre-sweeping is normally carried out a few days in advance of cable installation and the width of pre-sweeping area is usually 10 to 20m [26], depending on actual site condition.

However, even sand waves are dredged, sand waves usually recover themselves. Examples can be found in Bisanseto Sea [20] and the North Sea [7, 23].

The Bisanseto navigation channel, which is a trunk channel connecting the eastern and the western Seto Inland Sea next to the Kagawa Prefecture, Japan, required maintenance dredging because of sand wave recovery causing inadequate navigation depth. Katoh et al. [20] used the bathymetry survey record to estimate the migration and growth of sand waves. The publication showed that the mean water depth at some locations of the channel had decreased yearly at an inversely exponential rate due to existence of sand waves, as shown in Figures 3.5a and 3.5b.

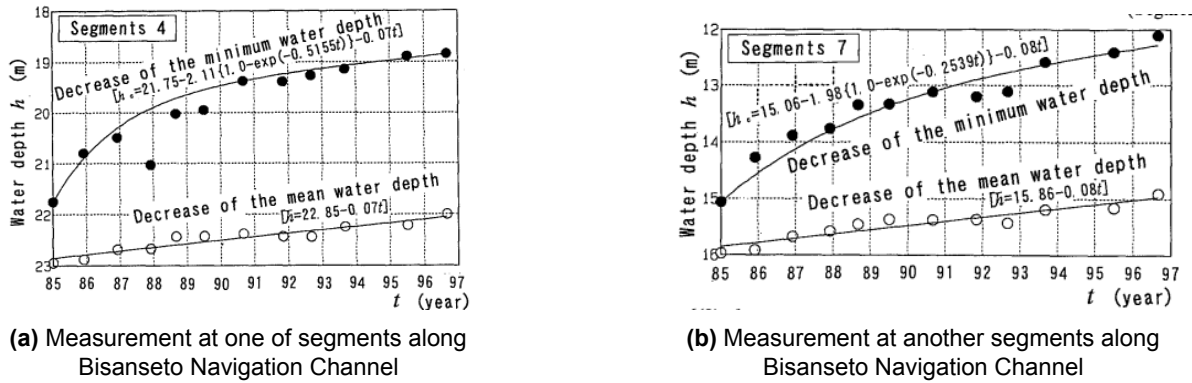


Figure 3.5: Empirical Model on sand wave recovery in Bisanseto Navigation Channel by Katoh et al. [20]

Another navigation channel, the Euro Channel to Rotterdam is also located in a sand wave field. Similar to Bisanseto navigation channel, sand waves reduce the navigation depth of the channel and maintenance surveying and dredging are regularly conducted. Through these measurement data, sand wave recovery was also identified in this channel [7].

Interestingly, sand wave recovery might not always happen (or might not happen within several years after dredging). Krabbendam et al. [23] studied the bedform development at the three local depressions on the Kwinte Bank and Buiten Ratel in the Belgian continental shelf of the North Sea. These local depressions were formed due to dredging activities. Based on the available bathymetry record at different locations, sand waves were formed 5 years after dredging at one of the local depressions but there was no sign of sand wave growth at the remaining two depression locations, as shown in Figure 3.6. It was explained that the possible reasons were variations in local sand availability and mean water depth. Especially the local sand availability was found important as it was stated that from the observation of sand wave regeneration at that particular local depression the sand waves were originated from local reworking processes, which means that the sand was eroded in the troughs and deposited on the crests.

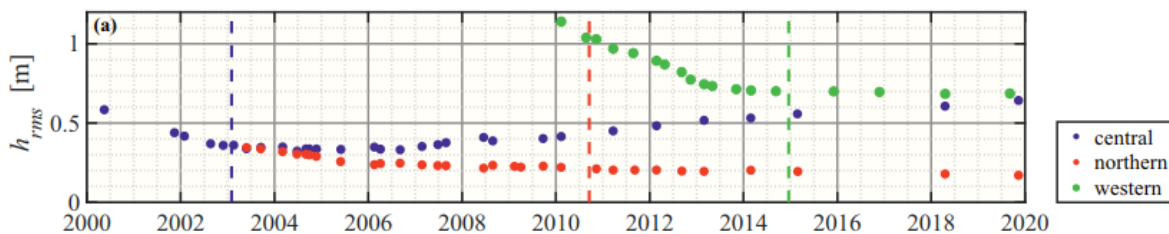


Figure 3.6: The Root-mean-square Bed Level at Three Local Depressions in Belgian North Sea [23]

In addition, in the vicinity of the local depressions analysed by Krabbendam et al. [23], an interaction between dredged and non-dredged areas was documented in other literature. Terseleer et al. anal-

used the dune migration in the Flemish Bank based on high-resolution bathymetry data [35]. In the publication, it is documented that the dunes surrounding the dredged area flattened when the sand waves within the dredged area were recovering.

These publications reveal the sand wave recovery processes after full dredging on a larger scale but publications related to sand wave recovery after cable trenching are scarce. In addition, these publications provided yearly development of sand wave recovery without any information related to the instantaneous bedform change after dredging. Nevertheless, a detailed bathymetry history after cable trenching in an offshore wind farm in the UK reveals the bedform change after cable trenching.

During the construction of the Race Bank Offshore Windfarm in the UK, extensive seabed surveys had been conducted to monitor the bedform change in days, weeks and months. The publications [30, 24] showed that during sand wave recovery there was an interaction between dredged and non-dredged areas. For example, lowering in the surrounding and bifurcation were observed in the vicinity of the pre-sweeping areas as shown in Figures 3.7a and 3.7b. Thus, sand wave recovery is demonstrated not a purely 2D problem, but 3D.

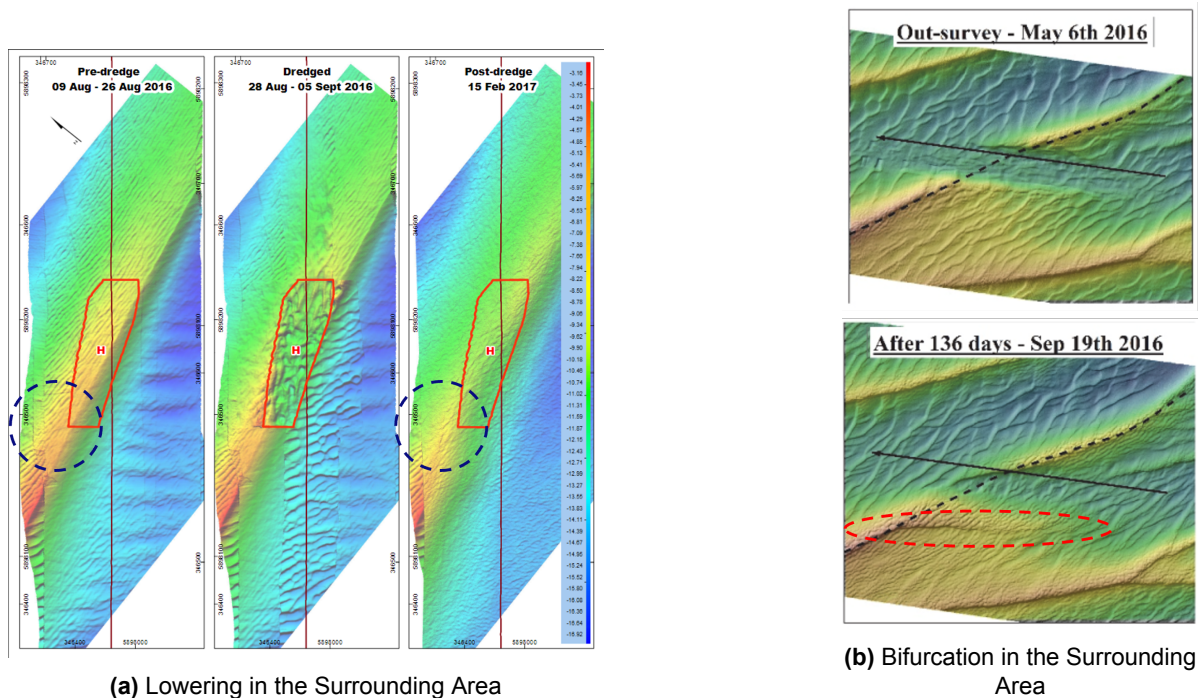


Figure 3.7: Observations on Interaction between Dredged and Non-dredged Area (Left: Observable Lowered Elevation in the Surrounding [30]; Right: Bifurcation Occurred in the Non-dredged Area [24])

In the meantime, from the observation at two locations in the offshore windfarm [24], it was discovered that regeneration of sand waves was limited in the first phase, namely “adaption period”, and this adaption period lasted 30 days and 87 days respectively at two locations. After the adaption period, it was named as “regeneration period” in which the regeneration of sand waves follows an asymptotic exponential form in this period, as shown in Figure 3.8.

According to the publication [24], a qualitative explanation of these two distinctive periods is provided. During the adaption period, there are limited regeneration and formation of megaripple in the trench area. In addition, although there is a slight adjustment on the trench slope but the trench area remains relatively unaffected. On the other hand, the regeneration period refers to the period when the sand wave is under regeneration and the net volume of backfill increases. However, these two distinctive periods are not documented in any other publications. A possible reason is that as the past publications focused more on the yearly development of sand wave regeneration, the adaption period, which has a time scale of only weeks or months as shown in the literature [24], was not able to be observed.

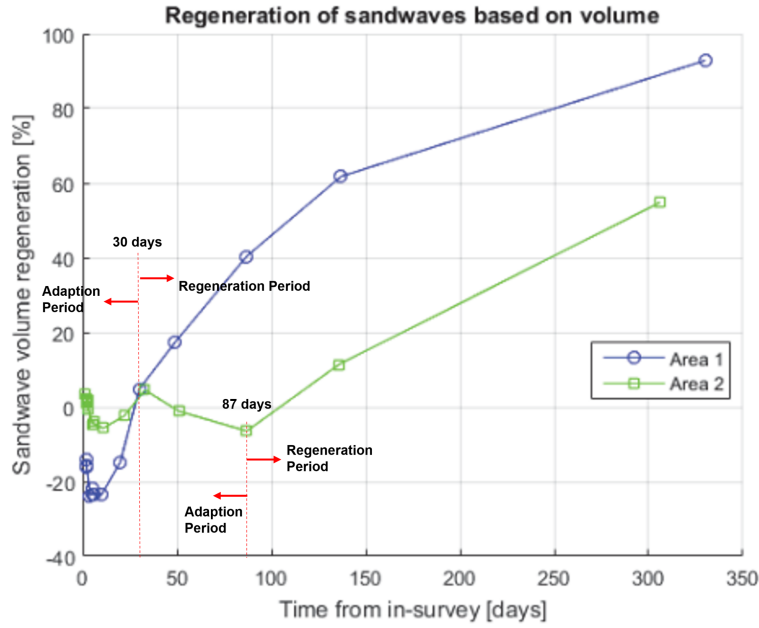


Figure 3.8: Sand Wave Regeneration in Percent at Two Areas in the Race Bank Offshore Windfarm [24]

In short, the occurrence of sand wave recovery depends on the local sand availability and possibly involves an interaction between the non-dredged area and the dredged area. During the sand wave recovery, two stages with distinct behaviour were observed. However, the physical explanation of the morphodynamics causing such an interaction or the two-staging development is not well understood.

3.2.2. Modelling sand wave recovery

In the past, literature adopted simple empirical or mathematical models to quantify the amplitude of sand wave recovery for a large-scale dredging. For example, as mentioned above, Katoh et al. [20] analysed measurement data recorded at Bisanseto Navigation Channel and formulated an empirical formula to estimate the rate of recovery. The only variable involved in the estimation is the time scale after dredging as shown in Figure 3.5. However, this simple approach involves no physical explanation of the phenomena and purely relies on available measurement data. As such, its applicability is limited.

Later, Hulscher developed a simple model [17] based on an analogy to a model for small ripples under sea waves proposed by Blondeaux [4] to estimate regenerated sand wave height. This simplified model assumes the sand waves are sinusoidal shaped and non-migrating and are developed from small-amplitude perturbations. It is derived that the height of the regenerated sand wave is dependent on the time and spatial location as shown in the formula below. This method requires measurement of existing perturbations wavelength and amplitude. Later, Hulscher incorporated her simple model with a genetic algorithm in order to improve the calibration in the site-dependent parameters, α_1 and α_2 .

$$\frac{h}{H} = A \cos(2\pi x/L) \quad (3.8)$$

$$\frac{\partial A}{\partial \tau} = \alpha_1 A + \alpha_2 A^3 \quad (3.9)$$

where h is the elevation change during recovery, H is the undisturbed water depth, A is the sand wave amplitude, x is the spatial coordinate, L is the wavelength of sand wave and τ is the morphological time scale.

However, such a method requires site measurement data for the calibration and the assumed 2D sinusoidal shape is unable to represent the actual sand waves shape. It is found that such a formula was a good estimation of the amplitude of sand wave recovery but overestimated the recovery time through a comparison between results from a 2DV process-based model and from the Hulscher's model [7]. Also, it was found that sand wave recovery depended on sand wave shapes, which is not included in the Hulscher's model [7].

Additionally, these models focused on the dredging of a whole sand waves field and the extent of dredging was totally different from a pre-sweeping case. In the meantime, as explained in the previous section, interaction between dredged and non-dredged area is documented in the literature but this interaction is not included in these models. Therefore, the application of the above simple models on sand wave recovery is debatable.

Nowadays, process-based morphological modelling is now commonly involved to study morphological evolution. For instance, Campmans et al.[7] modelled sand wave recovery after different dredging approaches by a 2DV process-based model on Delft3D. These existing process-based models were a 2DV model which implies that the processes involved in the model are restricted to the longitudinal direction of sand waves. Any interaction between dredged and non-dredged areas was not considered in these models, which does not fully represent the complete process of sand wave recovery as documented in other publications.

3.3. A Process-based Model - Delft3D FM

Delft3D FM is a process-based model containing several modules for hydrological, hydrodynamic and morphological modelling and it is also a successor of Delft3D 4. The major feature of Delft3D FM is an unstructured flexible computational grid, while Delft3D 4 relies on a structured grid. As a result, Delft3D FM allows a higher flexibility in the grid shape and size. It is found that Delft3D FM can model sand wave dynamics with an increased modelling efficiency [31], and thus, it is expected that utilising Delft3D FM could also improve the efficiency in modelling sand wave recovery.

In a numerical model incorporating both hydrodynamic and morphological modelling, there is a computation loop as shown in Figure 3.9[33]. This computation loop includes three parts: hydrodynamic modelling, sediment transport modelling and bed level updating. Within one computational time step, the hydrodynamics is firstly calculated, followed by the associated sediment transport. Finally, the bed level is updated due to net fluxes of sediment transport and affects the hydrodynamics in the next computational time step. Detail on each component is deliberated in the following sections.

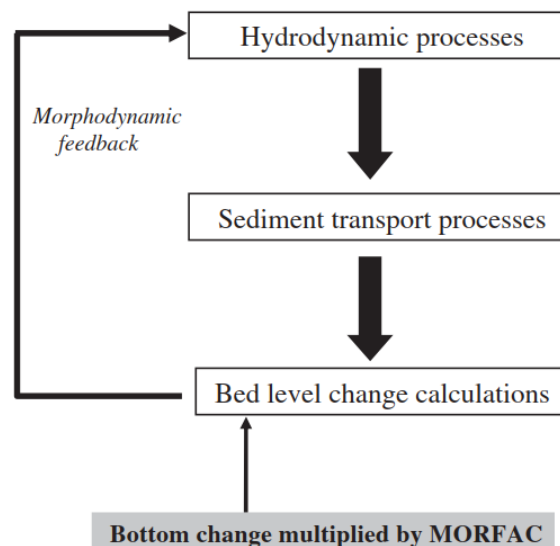


Figure 3.9: Computational Loop in Each Time Step (Reproduced from Ranasinghe et al. [33])

3.3.1. Hydrodynamic Modelling

Flow Equations

D-FLOW FM is a module in Delft3D FM calculating hydrodynamics by solving the continuity equation and the shallow water equations with assumptions of incompressible fluid, hydrostatic pressure and the Boussinesq assumption. The equations are expressed below:

Continuity Equation:

$$\frac{\partial h}{\partial t} + \frac{\partial uh}{\partial x} + \frac{\partial vh}{\partial y} = 0 \quad (3.10)$$

Navier-Stokes Equation:

$$\frac{\partial u}{\partial t} + u \frac{\partial u}{\partial x} + v \frac{\partial u}{\partial y} + w \frac{\partial u}{\partial z} - fv = \frac{-1}{\rho_0} \frac{\partial P}{\partial x} + F_x + \frac{\partial}{\partial z} (\nu_v \frac{\partial u}{\partial z}) + M_x \quad (3.11)$$

$$\frac{\partial v}{\partial t} + u \frac{\partial v}{\partial x} + v \frac{\partial v}{\partial y} + w \frac{\partial v}{\partial z} + fu = \frac{-1}{\rho_0} \frac{\partial P}{\partial y} + F_y + \frac{\partial}{\partial z} (\nu_v \frac{\partial v}{\partial z}) + M_y \quad (3.12)$$

Hydrostatic Pressure Assumption:

$$\frac{\partial P}{\partial z} = -\rho gh \quad (3.13)$$

where u , v and w are velocity in x-, y- and z-directions, f is Coriolis parameter, $\partial P/\partial x$ and $\partial P/\partial y$ are pressure gradient, ρ is density of fluid, F_x and F_y are Reynolds stresses, ν_v is vertical viscosity and M_x and M_y are momentum due to external sources.

Turbulence Model

In modelling vertical turbulence, different models can be used in Delft3D FM to model the vertical turbulent viscosity, such as constant coefficient, algebraic eddy viscosity closure model, $k-L$ turbulence closure model and $k-\epsilon$ turbulence closure model. Since viscosity is a combination of a characteristic length scale and a characteristic velocity scale, with a unit of m^2/s , for example, $k-\epsilon$ model uses a combination of turbulent kinematic energy and dissipation to formulate turbulent viscosity as shown below.

$$\nu_v = c_\mu \frac{k^2}{\epsilon} \quad (3.14)$$

In terms of horizontal turbulence, Smagorinsky subgrid stress model is used in Delft3D FM for modelling the horizontal turbulent viscosity. Smagorinsky subgrid stress model utilises the size of the computational grid as a component of turbulent viscosity and is expressed as follows:

$$\nu_t = (C_s \Delta_f)^2 \sqrt{2S_{ij}S_{ij}} \quad (3.15)$$

where C_s is Smagorinsky constant, which is defined by users, Δ_f is grid size and S_{ij} is velocity gradient and can be expressed, for instance, as follows:

$$S_{uv} = \frac{1}{2} \left(\frac{\partial u}{\partial y} + \frac{\partial v}{\partial x} \right) \quad (3.16)$$

3.3.2. Morphodynamic Modelling

Sediment Transport Formulation

In modelling morphodynamics, another module in Delft3D FM, namely D-Morphology, is used to model the sediment transport coupled with the hydrodynamics. In D-Morphology, bed-load transport and suspended load transport can be modelled by a variety of sediment transport formulations, such as Engelund-Hansen (1967), Meyer-Peter-Muller (1948) and Van Rijn (1984, 1993 and 2007).

Several past publications focused on the applicability of different sediment transport models, such as Engelund-Hansen (1967) and Van Rijn (1993, 2007), on modelling sand wave dynamics. Choy [8] investigated the impact of different sediment transport formulations, Engelund and Hansen (1967), Van Rijn (1993) and Van Rijn (2007), to modelling results of sand waves growth in Delft3D, and it was concluded that the formation of tidal sand waves was highly dependent to the choice of sediment transport model. Different models strongly affected the size, shape and growth rate of sand waves [8].

Van Rijn formulation had been improved throughout the years and different versions have been adopted in different research publications. In accordance with the study by Choy [8], both van Rijn formulations in 1993 and 2007 showed similar results in wavelength, wave height, time scales and overall behaviour but it was found that the formulation of van Rijn (2007) had great promise in modelling offshore sand waves growth.

Engelund and Hansen (1967) formulation estimates the total sediment transport by using the shear stress. In numerical simulations carried out by Choy [8], the use of Engelund and Hansen formulation resulted in a very large sediment transport rate, and thus, extremely high sand waves in a short time. On the other hand, this formulation does not include a distinction between bed load transport and suspended load transport, which is possibly not able to simulate the dampening effect due to suspended load transport as mentioned in Section 3.1.2.

Bed Slope Factor

As explained in Section 3.1.2, the slope of sand waves affects the bed-load transport, this factor is included in Delft3D FM by implementing a bed slope factor in the sediment transport vector.

$$S'_b = \alpha_s S'' \quad (3.17)$$

where S'_b is the adjusted bed-load transport vector due to the slope effect and S'' is the unadjusted bed-load transport vector calculated by different formulations without the slope effect.

The bed slope factor in the longitudinal direction is based on the study made by Bagnold [1] and deliberated as follows:

$$\alpha_s = 1 + \alpha_{bs} \left(\frac{\tan \theta}{\cos(\tan^{-1} \frac{\partial z}{\partial s}) (\tan \theta + \frac{\partial z}{\partial s})} \right) \quad (3.18)$$

where α_{bs} is a user-defined tuning parameter, θ is the angle of repose of the sediment, $\partial z / \partial s$ is the gradient of slope in the longitudinal direction.

On the other hand, the transverse slope induces an additional bed-load transport vector in the transverse direction and it is formulated as follows based on a study made by Ikeda [19]:

$$S_{b,n} = |S'_b| \alpha_{bn} \frac{u_{b,cr}}{u_b} \frac{\partial z_b}{\partial n} \quad (3.19)$$

where α_{bn} is a user-defined tuning parameter, $u_{b,cr}$ is the critical velocity at bed level, u_b is velocity at bed level and $\partial z_b / \partial n$ is the gradient of slope in the transverse direction.

Thus, the user is required to define the user-defined tuning parameters, α_{bs} and α_{bn} , in modelling the bed-load transport due to slope effects. In relation to the bed slope effect in the longitudinal direction, Overes [31] tested the influence of α_{bs} by sensitivity analysis. It was shown that this parameter prominently affects the growth rate and the shape of sand waves in a 2DV model by Delft3D FM. Choy [8]

also had a similar conclusion through sensitivity analysis and suggested that this parameter can be calibrated by the actual growth rate of sand waves. On the contrary, since the past publications focused on sand waves growth and migration or sand wave recovery in a 2DV model, sediment transport along the transverse direction and α_{bn} were not a concern. Thus, no information related to α_{bn} on the application of sand waves can be provided by past publications.

Bed Level Updating

With known sediment transport at a controlled area, the bed level at the controlled area adjusts due to Exner equation.

$$(1 - \epsilon_p) \frac{\partial z_b}{\partial t} + \frac{\partial S_{b,x}}{\partial x} + \frac{\partial S_{b,y}}{\partial y} = 0 \quad (3.20)$$

where ϵ_p is the bed porosity, z_b is bed level and $S_{b,x}$ and $S_{b,y}$ are sediment transport in two horizontal directions.

This Exner equation formulates the bed level at a controlled area with the net sediment fluxes from all directions into the area. If there is a net import of sediment into the area, the bed level rises. On the contrary, the bed level drops.

Morphological Time Scale Factor

Morphological Time Scale Factor or Morphological Acceleration Factor (which are usually referred as MORFAC or MF) is one of upscaling techniques to reduce computational time in morphological modelling. By applying MORFAC, the speed of change in morphology is expedited, and thus, inducing a significant impact to hydrodynamics.

In D-Morphology, the MORFAC is applied on the net erosion and deposition fluxes at each computational time step [12] as illustrated in Figure 3.9. For example, if MORFAC is applied as 10 in modelling morphological development under one period of tidal motion, this is equivalent to the morphological development under 10 periods of the tidal motion. Thus, applying MORFAC can result in a significant reduction in computational time.

Although the application of MORFAC can reduce computational time significantly and is convenient in long-term morphological modelling, it could lead to an unreliable result if the MORFAC is higher than a certain value, namely "critical MORFAC". Critical MORFAC is the highest MORFAC which provides a morphological prediction similar to a benchmark at an identical morphological time [33]. Since this upscaling technique assumes the morphological response is linearly proportional to hydrodynamic forcing in one morphological time step, a high value in MORFAC might violate this assumption and provide unrealistic results or computational instability, depending on the forcing [33].

Although critical MORFAC was studied by Ranasinghe et. al [33] with a simple case of unidirectional flow over symmetric bed perturbation and a guidance on selecting the critical MORFAC was provided, it was advised that the provided guidance might not be applicable directly to real life situation and the critical MORFAC depended on the morphology and forcing of the situation. It was still recommended to assess the validity of selected MORFACs by a sensitivity test.

Reviewing the models in the past publication simulating sand wave dynamics, a general picture on selection of MORFACs can be made. Krabbendam et. al [22] carried out a sensitivity analysis on MORFAC for the hindcast and forecast of the tidal sand waves evolution in the North Sea and tested MORFAC with values of 37, 74 and 148. Choy [8] compared results with 50 and 600 in MORFACs and found negligible differences in modelling sand waves growth. Tonnon et al. [36] simulated the morphological behaviour of an artificial sand wave in the North Sea and found that MORFAC can be up to 500 without affecting hydrodynamics and morphodynamics in an offshore area where the water depth is larger than approximately 15m. Van Gerwen [37] simulated sand waves growth until equilibrium and adopted 2000 in MORFAC.

From the above, it is noted that MORFACs adopted in the past publication varied from 37 to 2000 and it is claimed that larger MORFAC had negligible deviation from lower MORFAC. However, it is noted that these models were 2DV model and mainly simulated sand waves growth. The MORFACs adopted

in these models might not be necessarily applicable to a 3D model in sand wave recovery since the critical MORFAC depended on actual situation as concluded by Ranasinghe et. al [33].

4

Case Study - NEMO Link

4.1. Background Information

In this thesis, a case study, namely NEMO Link, is involved to study sand waves recovery in a real case and test the ability of Delft3D FM in modelling sand waves recovery. This chapter describes observations found in the bathymetry measurement record.

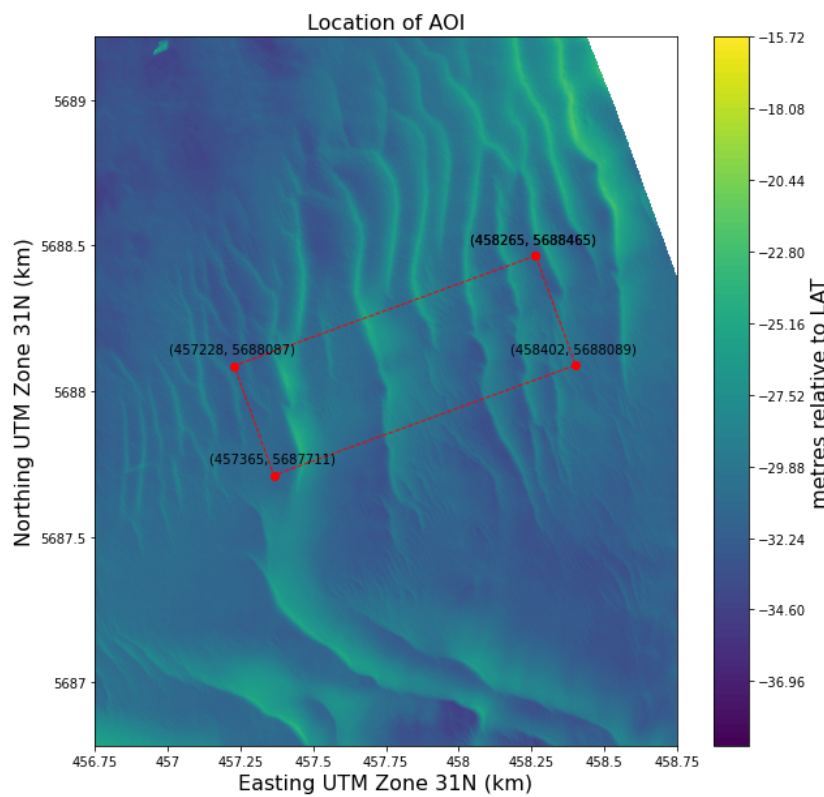
NEMO Link is a submarine cable connecting the electricity grids in the UK and Belgium and was constructed in 2018 by Siemens Energy. It is approximately 140 km long in total, including a submarine section of approximately 130km long. According to the Environmental Statement of the construction project [26], sand waves were identified at several locations before construction and proposed to be pre-swept.

One of these locations was selected as a case study, as shown in Figure 4.1, based on data availability and characteristics of local sand waves dynamics and was named as the Area of Interest (AOI). The AOI is 1100m long in the longitudinal direction, approximately 200m wide in the transverse direction and aligned along 255°N. From the open source dataset, EMODnet, bathymetry measurement data in November 2016, March 2018 and July 2021 were available. However, data in 2016 and 2021 has a higher resolution, with 1m x 1m, whereas the data in 2018 has a lower resolution, with 20m x 20m. Thus, only 2016 and 2021 datasets were chosen for analysis.

Although there is no data available on EMODnet showing the bathymetry condition immediately after dredging, a trench of 20m in lower width with 1/5 slope at sides was assumed in the Environment Statement of the project [26].



(a) Alignment of NEMO Link



(b) Coordinates of AOI

Figure 4.1: Location of NEMO Link and AOI

In this area, based on available information [26], pre-sweeping was carried out in early 2018 and a trench was formed for laying the submarine cable. Five sand waves were identified along the transect as shown in Figure 4.2. The crests of these sand waves were aligned between 143 to 175° N, approximately 80 to 112° to the centreline of the transect. Among these five sand waves, sand wave No.3 is a tail of a sand wave with decreasing wave height across the extent of the AOI. Sand wave No. 1 has a similar wave height to sand wave No. 2. Thus, sand waves No. 2, 4 and 5 were selected for further study on the characteristics of sand waves recovery.

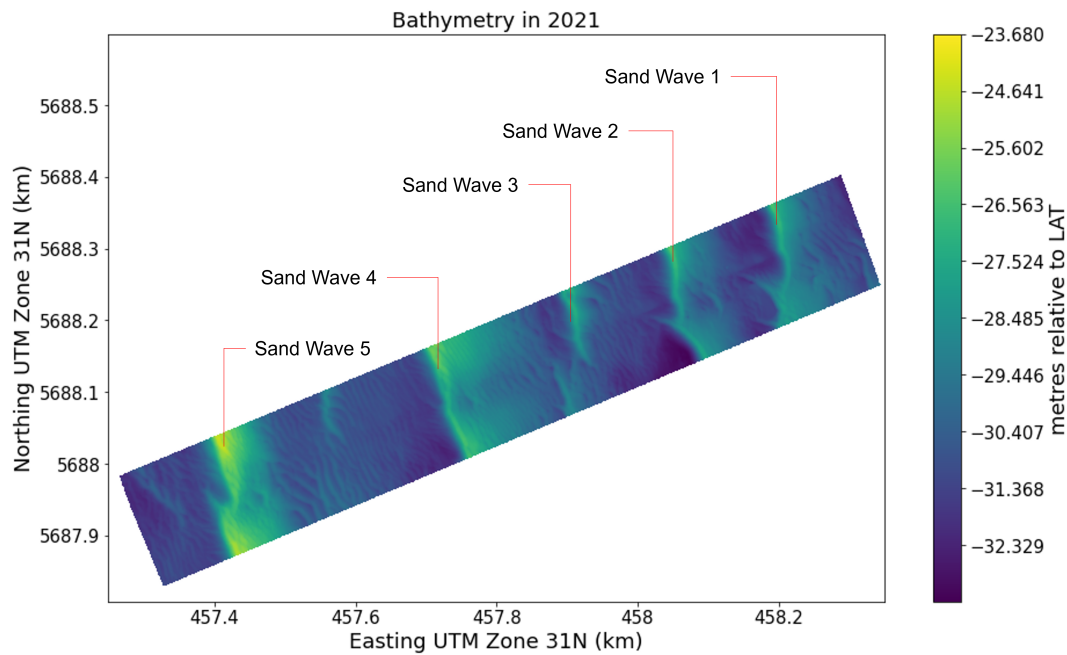


Figure 4.2: Sand Waves in the AOI in 2021

4.2. Hydrodynamic Condition at the AOI

The hydrodynamic conditions at the AOI were derived from Dutch Continental Shelf Model (DCSM) established and validated by Deltares [41], which includes the Southern North Sea, estuaries in the Netherlands and the Wadden Sea.

The ocean current at the AOI was hindcasted in the period of June 2016 without meteorological forcings. In general, the tidal current flows along the Northeast and the Southwest direction as shown in the scatter plot of Eastward versus Northward velocity in Figure 4.3. Further, the tidal residual current and the maximum current during this period were also identified and tabulated in Table 4.1.

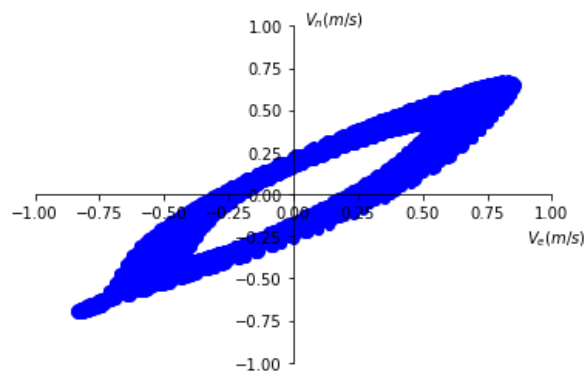


Figure 4.3: Scatter Plot of Eastward Versus Northward Velocity

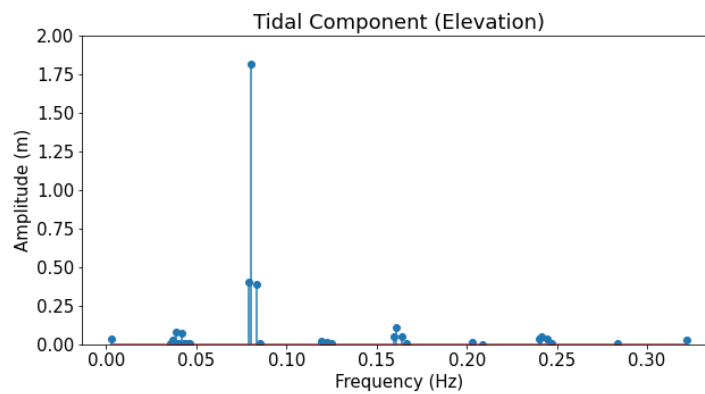
Vector	V_e (m/s)	V_n (m/s)	Magnitude (m/s)	Direction ($^{\circ}$ N)	Angle to Mean Sand Wave Crest Orientation ($^{\circ}$ N)
Maximum Vector	-0.85	-0.71	1.11	230	75
Residual Current Vector	0.02	0.02	0.03	44	64

Table 4.1: Flow Characteristics at AOI

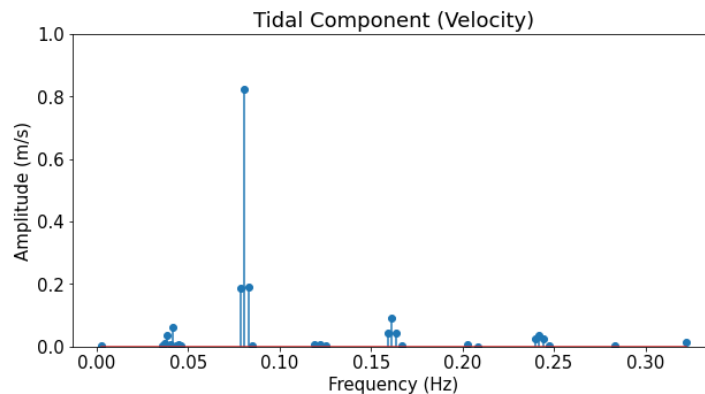
The tidal components of the tidal forcing were also identified by using a Python Package, TTide. It is noted that the four largest tidal components are M2, S2, N2 and M4 as shown in Figure 4.4, with their respective amplitude, period, phases and inclination as tabulated in Table 4.2.

Tidal Component	M2	N2	S2	M4
Frequency (Hz)	0.081	0.079	0.083	0.161
Period (hr)	12.42	12.66	12	6.21
Elevation Amplitude (m)	1.82	0.41	0.39	0.11
Elevation Phase Angle (deg)	58	303	302	59
Major Axis of Velocity Amplitude (m/s)	0.82	0.19	0.19	0.09
Minor Axis of Velocity Amplitude (m/s)	0.14	0.03	0.03	0.00
Velocity Phase Angle (deg)	94	340	337	82
Ellipse Inclination ($^{\circ}N$)	52.6	52.2	52.5	53.0

Table 4.2: Tidal Components at AOI



(a) Tidal Components Analysed by Water Elevation



(b) Tidal Components Analysed by Major Axis of Velocity Components

Figure 4.4: Tidal Components at AOI

Figure 4.5 shows the water elevation and velocity signals due to the M2 tidal constituents. It is shown that it is a propagating wave since the phase difference between the water elevation and the velocity is small.

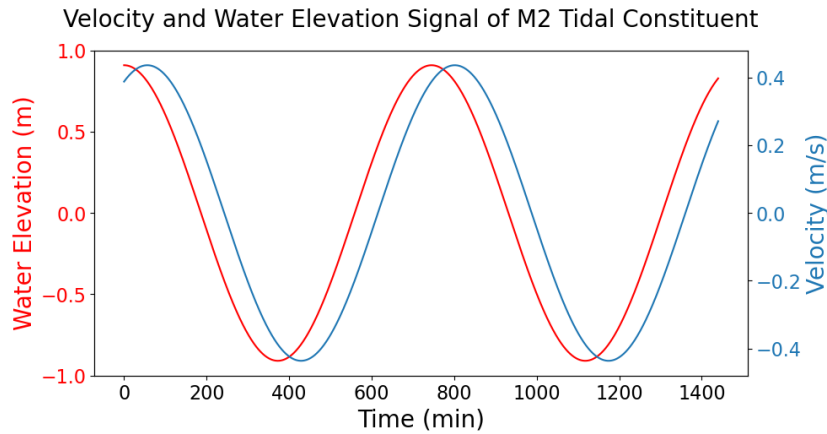


Figure 4.5: The Phase Difference between Water Elevation and Velocity due to M2 Tidal Constituent

The phase lag between M2 and M4 tidal constituents is analysed. It is explained that the presence of a higher tidal constituent, M4, contributes loss of symmetry of the circulation cell. This results in residual sediment transport due to the non-linear relationship between the flow velocity and the sediment transport [3]. In the publication [3], it is found that if the phase shift between M2 and M4 tidal constituents is between 30° and 180° , an upstream migration is induced [3]. From Table 4.2, the phase shift between M2 and M4 tidal constituents (i.e. $\phi_{M4} - 2\phi_{M2}$) is -106° or 254° , which indicates a downstream migration. Figure 4.6 shows the resultant velocity due to the M2 and M4 tidal components.

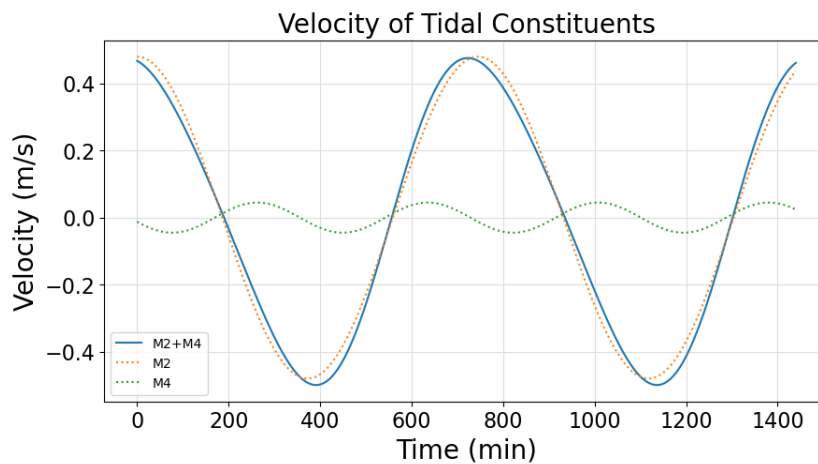


Figure 4.6: Velocity due to M2 and M4 Tidal Constituents

4.3. Sand Wave Characteristics

4.3.1. Analysis Methods

Transects along the centreline of the cable trench and 30m away from both sides of the centreline of the cable trench, total three numbers of transects were considered. The centreline transect provides information related to the sand waves in the dredged area, whereas the transects 30m away from both sides of the centreline provide information related to the sand wave in the non-dredged area. The 30m distance is chosen by consideration of the dimension of the trench as mentioned in Section 4.1.

In interpreting the measurement data, a sand wave should be firstly defined. In this thesis, the peak and trough of a sand wave refer to the local maximum and minimum of a sand wave respectively and the wavelength of each sand wave should be at least 100m to fulfil the common features of observed sand waves. To locate a sand wave, a Python package, Scipy, was firstly used to locate the local

maximum and minimum in every 125m along the transect. In other words, the separation between peaks or troughs should be at least 125m. Such distance was chosen in order to capture reasonable local maximum and minimum by the algorithms. Followed by defining peaks and troughs in the data, redundant local maximum and minimum were filtered manually to locate the unique peak and trough of concerned sand waves. Such a method could not accurately capture the troughs of sand waves in every circumstance because of fluctuations in signals. Nevertheless, this method is able to capture the peaks correctly and provides an efficient and reasonable estimation of the sand wave height.

In the meantime, the definitions of various sand wave characteristics from Krabbendam et al. [22] are adopted. Sand wave height is defined as the elevation difference between a peak and a trough of a sand wave and crest migration means the distance difference between the same peak at two different times. Figure 4.7 demonstrates different characteristics of a sand wave.

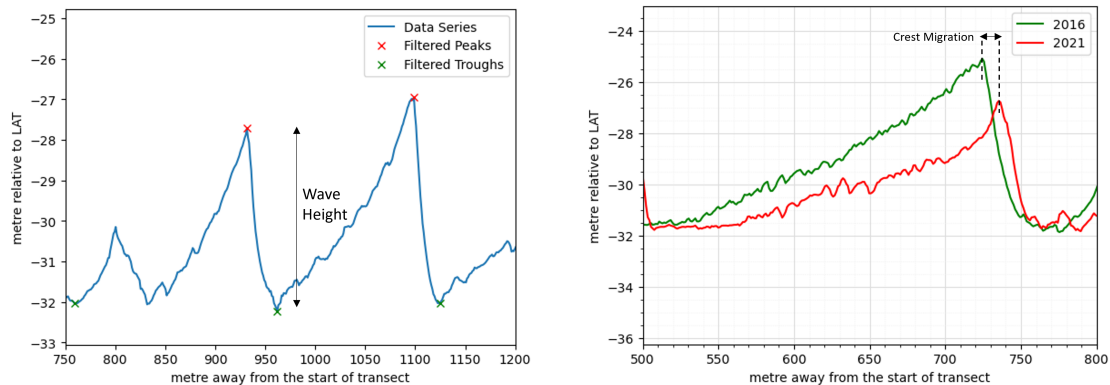


Figure 4.7: Definition of Sand Waves Characteristics

Apart from these features, sand waves will also be characterised by their shape, such as their slope and skewness.

To characterise the shape of a sand wave, a sand wave can be disintegrated into different parts, including the peak, the two troughs, the leeside and the stoss side.

However, there was an inconsistency in the definition of the leeside and the stoss side of a sand wave among different literature. For example, in the publication from Knaapen [21], the leeside refers to the side of a sand wave with a longer distance between the peak and the trough and the stoss side is another side with a shorter distance between the peak and another trough. However, in the publication from Damen [11], the definition is the other way around.

In view of the analogy to a river dune and the preferred direction of sand wave migration, in this thesis, the following definition was adopted. The stoss side refers to the side of a sand wave with a longer distance from the peak to the trough and with a gentler gradient and also the upstream side of sand wave migration. On the other hand, the leeside refers to the side of a sand wave with a shorter distance from the peak to another trough and with a steeper gradient and also the downstream side of sand wave migration. To schematically illustrate these, Figure 4.8 refers.

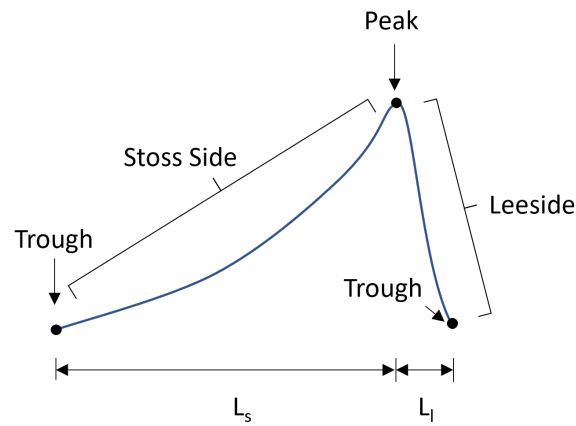


Figure 4.8: Terminology in a Sand Wave

As such, it was defined that the sand wave asymmetry has the following formulation:

$$A = \frac{L_s - L_l}{L} \quad (4.1)$$

where A indicates asymmetry of a sand wave, L_s is the length of the leeside of a sand wave, L_l is the length of the stoss side of a sand wave and L is the sum of these two lengths.

4.3.2. Sand Wave Height

As shown in Table 4.3, the height of different sand waves was similar in the transverse direction in 2016. Due to the fact that dredging activity was carried out in 2018, the sand waves had recovered from 2018 to 2021 but have yet to reach their original height. Outside the dredged area, an obvious decrease in sand waves height was observed at 30m away from the centerline in 2021. The sand wave height dropped approximately 1 to 2m on the Northern side and 1 to 3m on the Southern side. From the available data, an elevation drop was observed until 90m away to the North of the centreline and 105m away to the South of the centreline, which implies that the area of influence could be up to 200m wide.

The sand waves height at the centerline and 30m away from the centerline of the concerned sand waves are tabulated in Table 4.3.

Year	Sand Wave No.2	Sand Wave No.4	Sand Wave No.5
Along Centreline			
2016	5.2	6.8	7.7
2021	3.5	4.4	5.5
Along 30m Away from the North			
2016	5.6	6.5	7.8
2021	4.4 (-1.2)	4.6 (-1.9)	5.6 (-2.2)
Along 30m Away from the South			
2016	5.0	6.3	8.2
2021	4.2 (-0.8)	5.0 (-1.3)	5.0 (-3.2)

Table 4.3: Sand Wave Height (m) along Different Locations
(Red numbers indicate the height difference)

4.3.3. Sand Wave Migration

The available data is limited to conclude the migration rate of the sand waves because the pre-sweeping perhaps affected the local hydrodynamics or morphodynamics. However, the peak locations of sand

waves can provide some information on sand wave migration in the AOI. In general, the sand waves migrated downstream (i.e. the Southwest direction) along the transect as indicated by the peak locations. In comparison with the hydrodynamic condition stated in 4.1, the migration of sand waves was possibly determined by the maximum flow or the phase lag between M2 and M4 tidal constituents, based on the direction of the flow and the migration.

From the data in Table 4.4, it is shown that the morphological movement on the Southern side of the transect was more dynamic and active than on the Northern side. The sand waves on the Southern side moved much faster than the Northern side.

Location	Sand Wave No.2	Sand Wave No.4	Sand Wave No.5
Along Centreline	8.7 (1.9)	17.4 (3.7)	4.3 (0.9)
30m Away to the North	6.5 (1.4)	8.7 (1.9)	-1.1 (-0.2)
30m Away to the South	13.0 (2.8)	17.4 (3.7)	28.2 (6.0)

Table 4.4: Migration Distance (m) and Average Migration Rate (m/yr) in Brackets of Sand Wave Peaks

(Positive values indicate movement to downstream and negative value indicates movement to upstream)

4.3.4. Recovered Sand Wave Shape

In identifying different parts of a sand wave, the same approach in identifying the peaks and troughs along the whole series is adopted but only related data series of a particular sand wave and a finer separation distance are used in order to precisely capture the unique peak and troughs of a sand wave. The sand waves with their peak and troughs along the centreline are shown in Figures 4.9a to 4.9c as an example. The characteristics of all three sand waves along the centreline and outside dredging area are tabulated in Tables 4.5 to 4.7. Consistently, the gradient of the leeside is between 7 to 10 degrees. In addition, they all have a skewness of around 0.7, except the part of sand wave No.2 outside the dredged area.

From the parameters shown in Tables 4.5 to 4.7, the recovered part of sand waves maintained a similar shape as in the non-dredged area. They had similar asymmetry, stoss side gradient and leeside gradient. The recovered and non-dredged parts of sand waves were asymmetrical and leaned towards downstream direction.

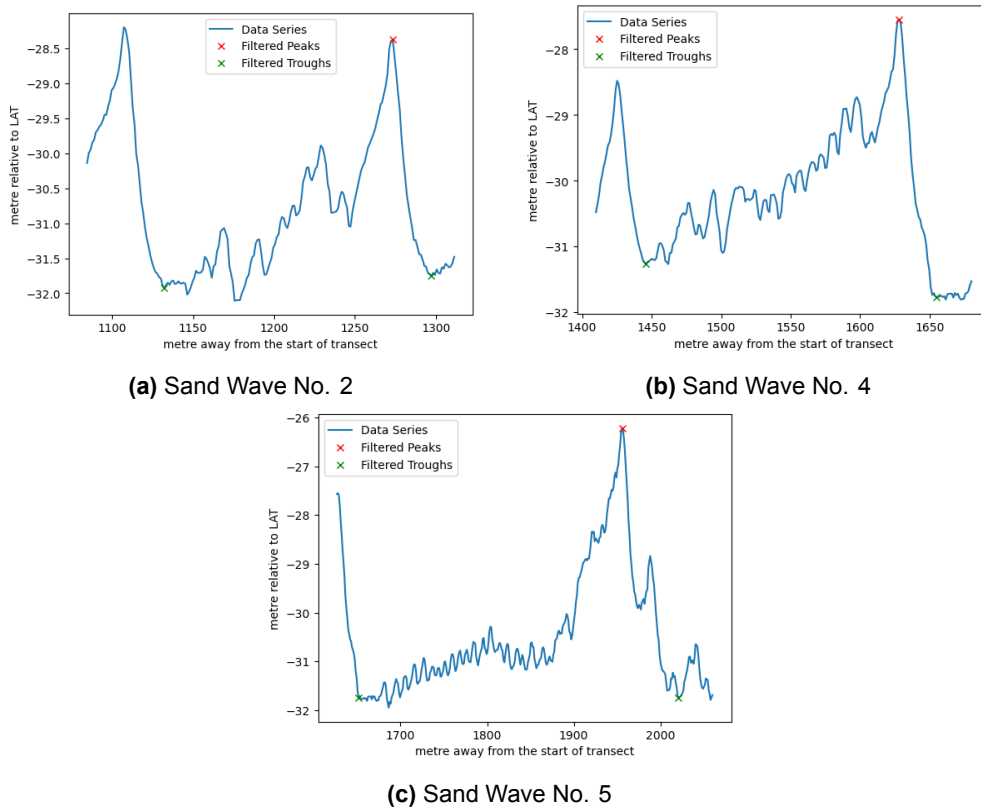


Figure 4.9: Elevation of Each Recovered Sand Wave and its Peaks and Troughs

Shape Parameters	Sand Wave No.2	Sand Wave No.4	Sand Wave No.5
L_s (m)	141	182	304
L_l (m)	24	27	65
A (-)	0.71	0.74	0.65
Stoss side Gradient (deg)	1.4	1.3	1.0
Leeside Gradient (deg)	8.0	8.8	4.8

Table 4.5: Shape Parameters of Sand Waves No. 2, 4 and 5 along Centreline in 2021

Shape Parameters	Sand Wave No.2	Sand Wave No.4	Sand Wave No.5
L_s (m)	134	163	287
L_l (m)	35	39	65
A (-)	0.59	0.61	0.63
Stoss side Gradient (deg)	1.9	1.6	1.1
Leeside Gradient (deg)	7.3	6.7	4.9

Table 4.6: Shape Parameters of Sand Waves No. 2, 4 and 5 along 30m Away from the Northern Side in 2021

Shape Parameters	Sand Wave No.2	Sand Wave No.4	Sand Wave No.5
L_s (m)	95	152	310
L_l (m)	25	26	46
A (-)	0.59	0.71	0.74
Stoss side Gradient (deg)	2.5	1.8	0.9
Leeside Gradient (deg)	9.5	10.3	6.3

Table 4.7: Shape Parameters of Sand Waves No. 2, 4 and 5 along 30m Away from the Southern Side in 2021

Particularly, at the development of sand wave No. 2 in detail as shown in Figures 4.10a and 4.10b, it was observed that the ridge of the sand wave was no longer consistent as in 2016. Two distinct sand wave tails were developed from the sides of the trench in 2021 because they showed different curvatures and the tails were aligned with the corresponding curvatures in the non-dredged area. Dredging activity in 2018 interrupted the consistent ridge of the sand waves and possibly left a scar leading to such behaviour.

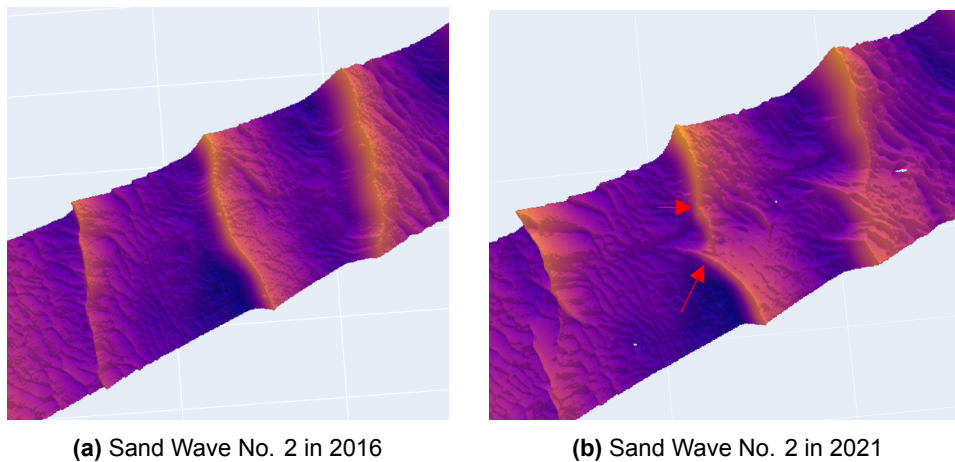


Figure 4.10: Recovery in Sand Wave No. 2

4.4. Sediment Budget

4.4.1. Analysis Methods

A sediment budget in the AOI was calculated and it was calculated based on the total sediment volume difference between two different times in particular zones. The AOI is divided into three different zones: mid-zone, which refers to the area of 15m offset from both sides of the centreline of the transect, upper zone, which refers to the area on the Northern side of the Mid-zone, and lower zone, which refers to the area on the Southern side of the Mid-zone. Figure 4.11 refers. The 15m offset distance is chosen based on an assumption of the trench geometry.

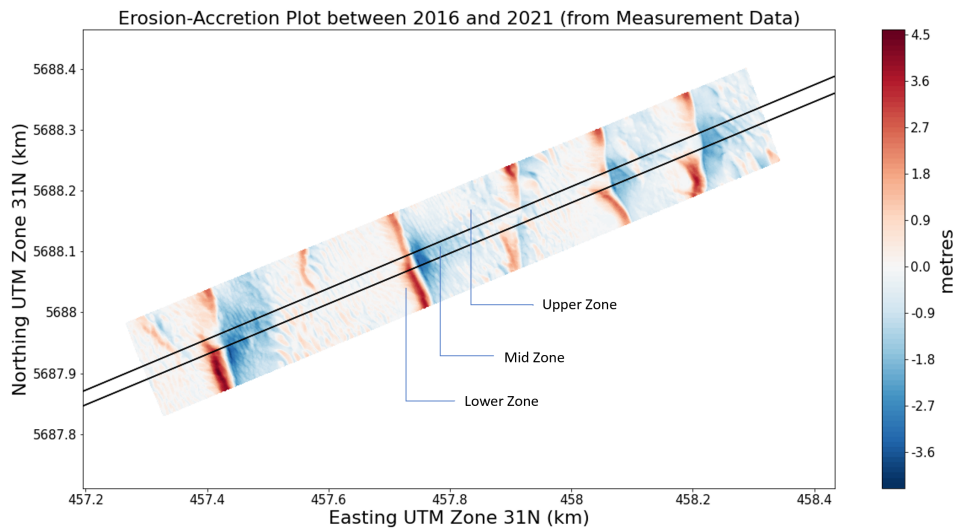


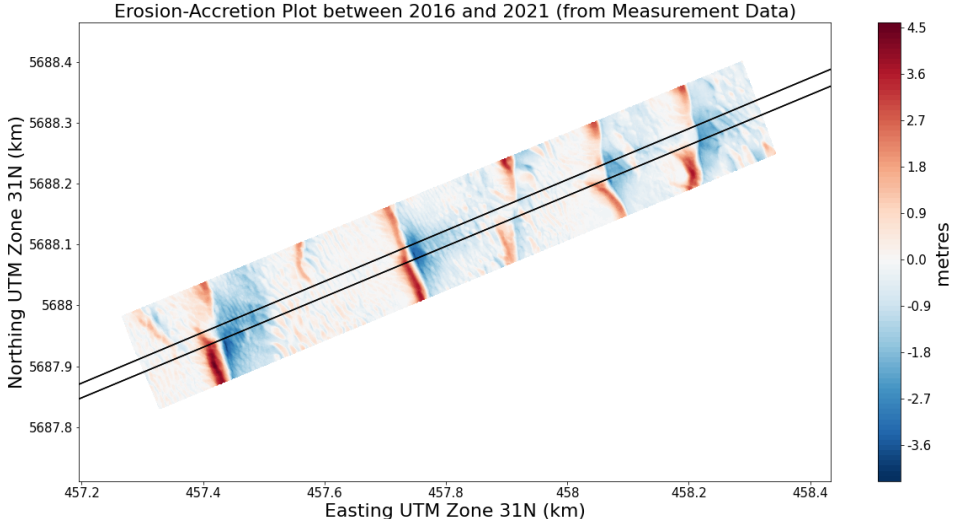
Figure 4.11: Extent of Each Zone

4.4.2. Results

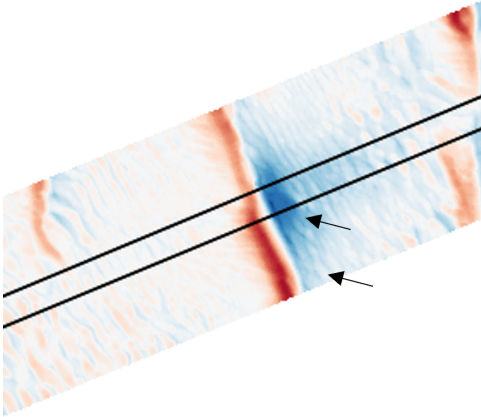
Figure 4.12a shows the elevation difference between 2016 and 2021 and erosion and accretion are indicated as blue and red respectively to show the sediment dynamics. In addition, the sediment budget difference in the AOI is tabulated in volume and also converted into an equivalent metre in elevation by dividing the sediment volume difference by the area of the corresponding zones as tabulated in Table 4.8.

In general, erosion is higher in the mid-zone consistently indicating the dredging activity in 2018. Also, the system had lost sediment after 5 years, which is consistent with the observation of a decrease in all sand waves height as shown in Tables 4.3 and the fact of dredging activity.

In addition, an interaction between dredged and non-dredged areas is observed after pre-sweeping. It is observed that there is a certain tendency in which erosion was larger in both magnitude and extent when the location was closer to the dredged area. Taking examples of sand wave no. 4 as shown in Figure 4.12b, the erosion, which is indicated by the blue colour, is more intense and larger in extent at the interface between dredged and non-dredged areas.



(a) General Picture of Erosion and Accretion Plot



(b) Erosion at Sand Wave No. 4

Figure 4.12: Erosion and Accretion Plot Between 2016 and 2021

Location	Sediment Budget in m^3	Sediment Budget in m
Upper Zone	-21,700	-0.27
Mid-Zone	-16,300	-0.62
Lower Zone	-16,800	-0.23
Total / In Total Area	-54,800	-0.30

Table 4.8: Sediment Budget of AOI in Volume (m^3) or in Equivalent Metre (m)

4.5. Summary

A location in the Southern North Sea is chosen for the case study due to the data availability and the morphodynamics. There were 5 sand waves at the location. In 2021, the sand waves height varied between 3m to 6m and the distance between two sand wave troughs varied between 160m to 360m. The sand waves crests were oriented towards 143 to 175 °N. With the aid of numerical modelling by the DCSM, the tidal condition at the location was hindcasted. The spring tide was towards the Southwest and the tidal-averaged residual current was towards the Northeast. Pre-sweeping was carried out in 2018 while the publicly available data of topography measurement was in 2016 and 2021. By a comparison between these two years data, the observations are noted as follows.

Sand Waves Migration

Migration of sand waves was observed based on the crest migration and the shape of sand waves. Table 4.4 shows that generally sand waves had positive migration distance indicating migration to the downstream, which is the Southwestern direction. This resulted in asymmetrical shapes of sand waves as shown in Figures 4.9a to 4.9c. The average migration rate of these five sand waves in the AOI is around 1.4m with a standard deviation of 1.5m. The reasons of the Southwestern migration are possibly due to the tidal asymmetry due to the phase lag between M2 and M4 tidal constituents or the spring tide.

Interaction between Dredged and Non-dredged Areas

Interaction between dredged and non-dredged areas was observed. From the sand wave heights and erosion-accretion plots, it was observed that the sand wave heights dropped in the area close to the pre-swept area after construction and the erosion-accretion plots indicated that the erosion was more severe as the location was closer to the dredged area. The elevation drop in the non-dredged area could reach 1 to 3m. These demonstrated that the surrounding of dredged area was also affected due to pre-sweeping. Such an area of influence could be up to 100m on each side along the transect.

Independent Recovery Behaviour

From the observation, it is noted that after pre-sweeping, the sand waves lost their consistency of ridge shape. From the observation in one of the sand waves, as shown in Figure 4.10, the recovered sand waves formed distinctive tails from the sides after dredging, and thus, lost the smooth profile on the leeside of the sand wave. The reasons of such features are unknown or possibly due to the dredging activity.

5

Numerical Modelling

This chapter deliberates on the configuration of the numerical model and the results from simulations. In the previous chapter, sand wave recovery and migration are observed from the bathymetry data. This numerical model aims to simulate the environment with tidal forcing and reproduce the phenomena, and thus, provides insight into the physical processes behind sand wave recovery.

5.1. Model Setting

5.1.1. Computational Grid and Vertical Discretisation

The computational grid, as shown in Figure 5.2, is a nested rectangular grid with an extent of approximately 3500m in the longitudinal direction and 4500m in the transverse direction.

The cell size of the computation grid varies from 2m x 5m (longitudinal dimension x transverse dimension) to 128m x 320m. The minimum cell size is determined based on the geometry of the trench and sand waves. Since the side slopes of the trench have a gradient of 1 to 5 based on the assumption in the Environment Statement of the project [26], the grid size in the transverse direction is adopted as 5m. In addition, in order to accurately simulate the shape of sand waves as shown in Figure 5.1, the cell size should be small enough to capture the profile.

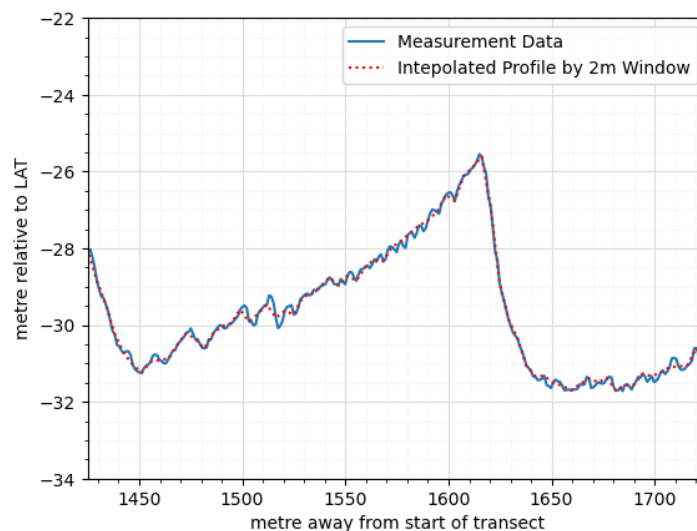


Figure 5.1: Comparison between Real Measurement Profile (Blue) and Interpolated Profile in the Model (Red Dotted Line)

The extent of the computational grid should be large enough to provide sufficient distance and avoid boundary effects. More than 1500m beyond the AOI is provided in the transverse direction and more than 750m beyond the AOI is provided in the longitudinal direction. The orientation of the computational grid is set as 250°N , which is perpendicular to the average sand wave crests orientation. The computational grid contains over 68,000 cells. For vertical discretisation, a sigma coordinate system of 40 σ -layer is used. Together with the number of cells in the computational grid, there are over 2.72 million cells in the computation at each time step.

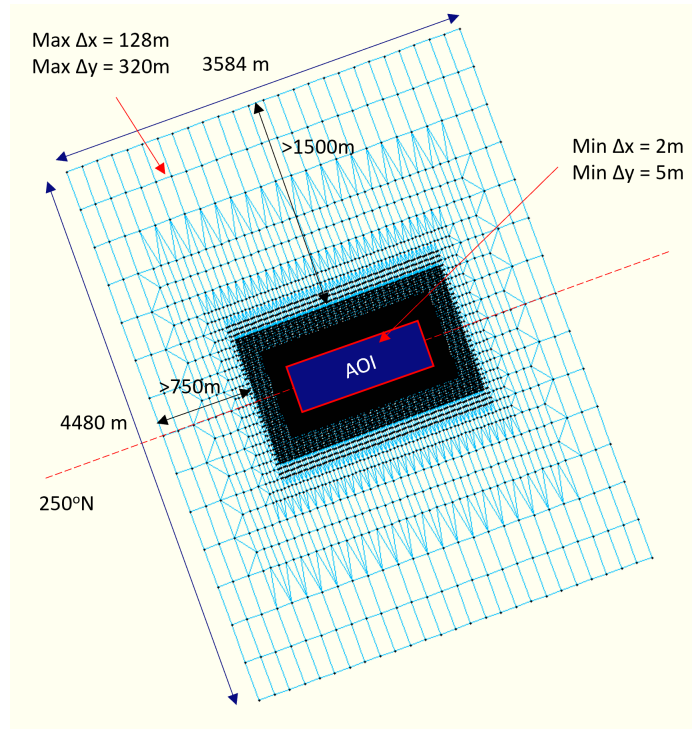


Figure 5.2: The Model Domain

5.1.2. Bathymetry

The bathymetry of the model consists of the dataset in 2016 with higher resolution (i.e. 1m x 1m) available on EMODnet and the bathymetry with lower resolution (i.e. approximately 840m to 930m) from the DCSM. In general, the bathymetry information of the model can be divided into three different areas, Areas A, B and C, as shown in Figure 5.3.

Area A mainly includes sand waves No. 1 to 5 as mentioned in Chapter 4 and a 150m buffer area, and full detail in topography from EMODnet is adopted with the finest grid cells in this area. Area C is an area with sufficient extent in order to reduce boundary effects on the flow to Area A and in this Area C, the bathymetry in the DCSM is adopted in the model. Finally, Area B is a transition area in which an additional factor is applied to smoothen the topography detail and merge a higher resolution bathymetry data to a lower resolution bathymetry data.

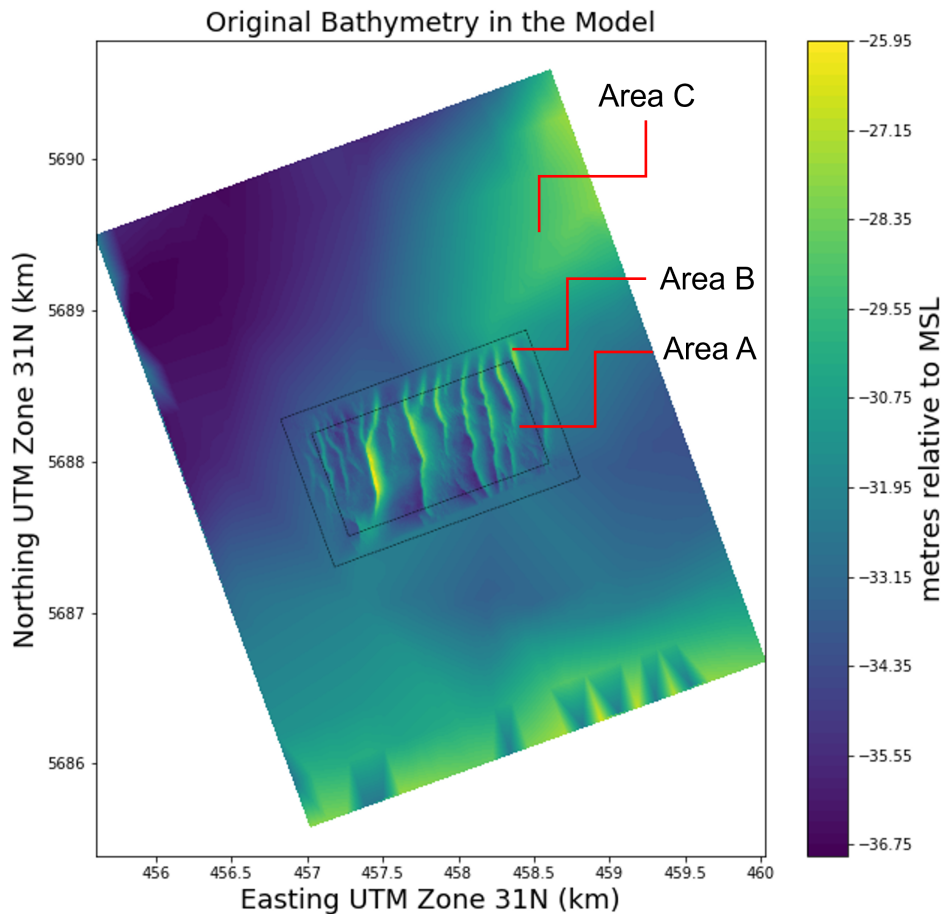


Figure 5.3: Bathymetry in the Model

Since the bathymetry measurement data from EMODnet and the bathymetry adopted in the DCSM have different reference levels, a conversion is required to make them consistent in the numerical model.

The bathymetry measurement data from EMODnet uses the lowest astronomical tide (LAT) as the reference level, whereas the bathymetry in the DCSM uses mean sea level (MSL) as the reference level. A conversion between LAT and MSL is necessary. The conversion is based on two bathymetry tiles available on EMODnet. These two bathymetry tiles provide bathymetry levels in the North Sea with respect to LAT and MSL respectively and are based on a numerical tide model, “Global Tide Surge Model” developed by Deltares [13]. This model simulates tidal forcing with consideration of other factors, including wind and surface pressure, such that the LAT at an area is modelled. Within the AOI, the difference between LAT and MSL is between 2.46m and 2.47m, and thus, 2.465m is taken as the conversion value.

5.1.3. Boundary Conditions

The type of boundary condition adopted in the model is an advection boundary condition. This type of boundary condition consists of water level and velocity profile over depth in both horizontal directions, as schematised by Overes in Figure 5.4. According to Overes [31], using this boundary condition is able to have a good representation of both water level and velocity in dealing with a small model area.

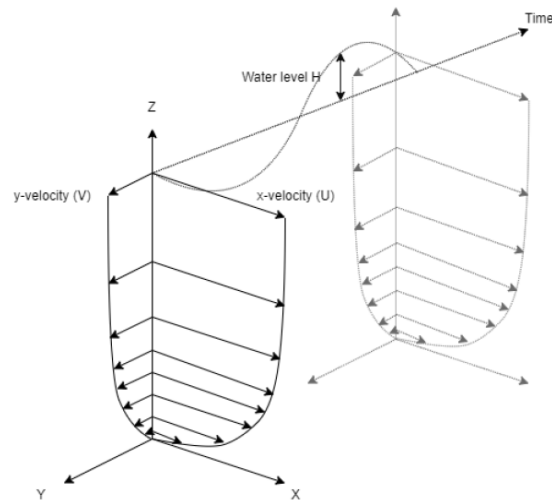


Figure 5.4: Illustration of an Advection Boundary Condition (Reproduced from Overes [31])

This type of boundary condition is applied to all boundaries of the model. The elevation and velocity information of the boundary conditions is extracted from June 2017 simulated by the DCSM. Since only tidal forcing is considered, the meteorological forcing in the DCSM was removed in order to obtain boundary conditions without such forcing.

5.1.4. Sediment Parameters

Verfaillie et al. attempted different geostatistic methods to interpolate the sedimentology at the Belgian Continental Shelf [40]. She utilised a sedimentological database from Renard Centre of Marine Geology, Ghent University, which includes information on samples obtained from the Belgian Continental Shelf, and a high-resolution digital elevation model from the Ministry of the Flemish Community to interpolate the distribution of median grain size at the Belgian Continental Shelf. The interpolated distribution of median grain size at the Belgian Continental Shelf by kriging with an external drift, which was proved more accurate compared with linear regression and ordinary kriging, from the publication is reproduced and shown in Figure 5.5. It is shown that the median grain size at the AOI was estimated between $350\mu m$ and $400\mu m$. A sensitivity analysis on these two median grain sizes, $350\mu m$ and $400\mu m$, was carried out and is deliberated in Appendix A. The analysis shows that the results between the two median grain sizes are negligible. As such, a sand material with $350\mu m$ in median sediment diameter (d_{50}) was adopted in the model.

5.1.5. Sediment Transport Formulation

Van Rijn (1993) formulation is adopted in the simulation. Both Van Rijn (1993) and (2007) were attempted in order to find an appropriate formulation for modelling sand wave dynamics and recovery at the AOI. It is found that Van Rijn (1993) formulation can maintain the shape of sand waves more, compared with Van Rijn (2007) formulation. Detail of the comparison is included in Appendix A.

On the other hand, the user-defined tuning parameters for the slope effect, as explained in Section 3.3.2, in the streamwise direction (α_{bs}) is set as 1.5. A sensitivity analysis on these two slope correction factors was carried out and is deliberated in Appendix A. It is found that if the slope correction factor in the streamwise direction is adopted as 3, the shape of sand waves becomes more dispersed. Thus, 1.5 is adopted as the slope correction factors in the streamwise direction.

For the parameters for the transverse slope effect (α_{bn}), it is set as 1.5, which is the default value in Delft3D FM.

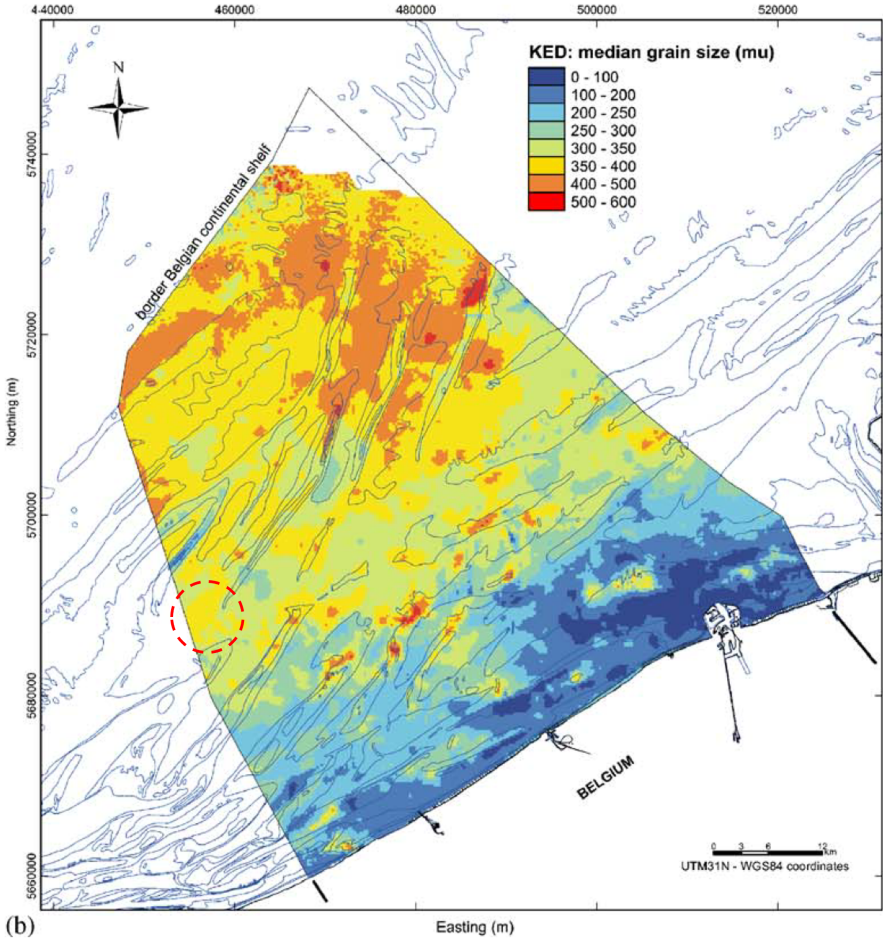


Figure 5.5: Median Grain Size Interpolated by Kriging with an External Drift [40] (The Circled Area is the Approximate Location of the AOI)

5.2. Hydrodynamic Performance of the Model

The hydrodynamic conditions in the numerical model were compared with the results from the DCSM. Figure 5.6 shows the velocity and water elevation time series at a point, which is the closest location to the AOI, with the same bathymetry as the DCSM. It is shown that water elevation and velocity matched with the DCSM quite well.

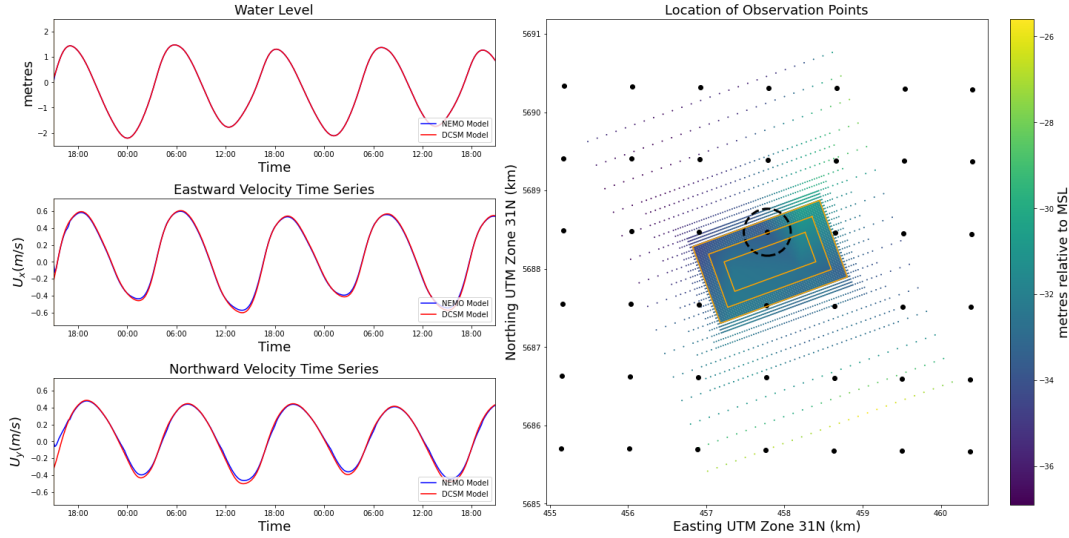


Figure 5.6: Comparison in Hydrodynamics between the Model and the DCSM

5.3. Simulation Scenarios

Two simulation cases, namely “pre-dredging case” and “post-dredging case”, were carried out by Delft3D FM 2022.03 Release. The pre-dredging case aims to simulate sand wave dynamics at the AOI before dredging and provide a general understanding of the Delft3D performance on modelling sand wave dynamics in a 3D setting. The post-dredging case aims to simulate the sand wave recovery process and provide insight into the hydrodynamics and morphodynamics of sand wave recovery, which is the focus of this thesis. With the results from the pre-dredging case, any observations which appear in both cases can be considered irrelevant to sand wave recovery.

The pre-dredging case simulates the sand wave dynamics in the AOI for 17 months from November 2016, which is the measurement time of the first bathymetry data, to April 2018, which is the month when the pre-sweeping was carried out. In order to have the same simulation period in the morphological time scale, the pre-dredging case was carried out with 100 in MORFAC and simulated under 10 tidal cycles. The post-dredging case continues the simulation based on the bathymetry obtained from the pre-dredging case but with 323 in MORFAC for 7 tidal cycles. The realtime duration is 39 months from April 2018 to July 2021, which is the measurement time of the second bathymetry data. The setting of the two simulation cases are summarised in Table 5.1.

The simulations were carried out on DelftBlue, an HPC cluster at Delft University of Technology. For each simulation, 32 numbers of cores were utilised. Together with the MORFACs, each simulation consumed less than 24 hours to achieve the required morphological time scale.

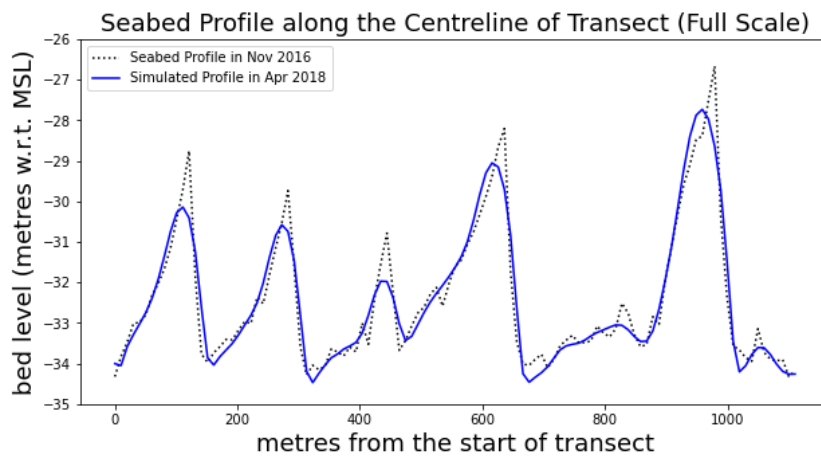
Scenario	Pre-dredging	Post-dredging
Simulation Time	Nov 2016 - Apr 2018	Apr 2018 - Jul 2021
Realtime Duration	17 Months	39 Months
MORFAC	100	323
Simulation Duration	10 Tidal Cycles	7 Tidal Cycles

Table 5.1: Settings of Simulation Scenarios

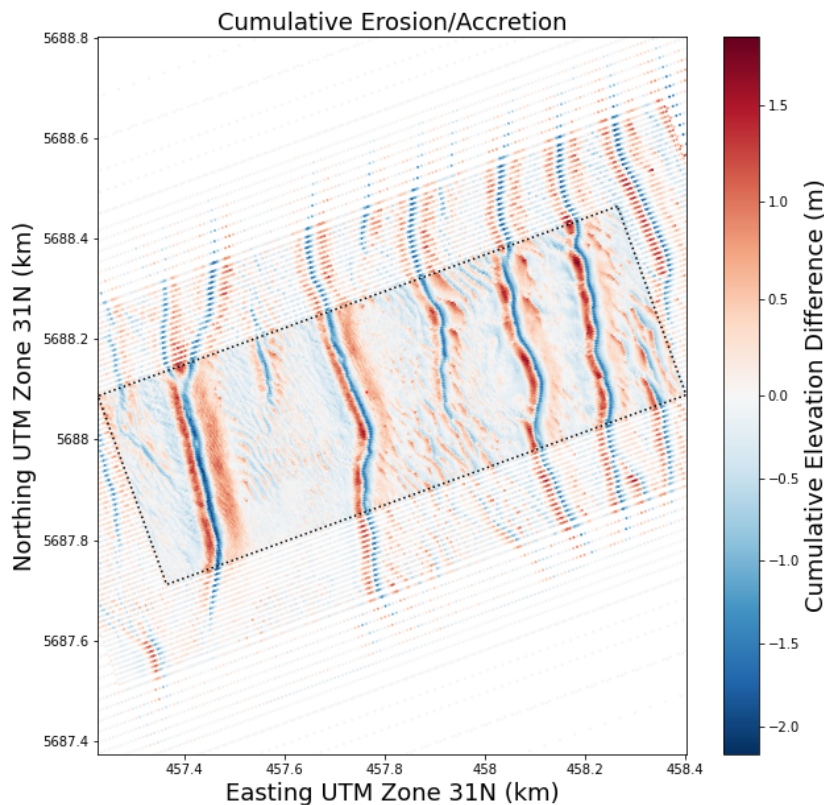
5.4. Simulation Results

5.4.1. Pre-dredging Case

The seabed profile along the transect and the erosion-accretion plot are shown in Figures 5.7a and 5.7b. It is shown that the current setting of Delft3D FM is unable to maintain the shape of sand waves accurately. From Figure 5.7a, it is shown that the model tends to smoothen all morphological features, including sand waves and megaripples. As a result, the peak elevation reduces by 1m. This is also demonstrated by the erosion at the sand wave crests as indicated by the blue regions and the deposition at leeside and stoss side of the crests as indicated by the red regions in the erosion-accretion plot.



(a) Simulation Result in Pre-dredging Case



(b) Erosion-accretion Plot in Pre-dredging Case

Figure 5.7: Results from the Pre-dredging Case Simulation

5.4.2. Post-dredging Case

Figure 5.8 shows the seabed elevation difference with respect to the mean seabed level along the centreline of the transect derived from the measurement in 2021 and the model result and it shows sand wave recovery. The mean seabed level is the mean topographic level along the transect in the measurement data or the model in order to make a comparison. The height of the simulated sand waves generally halves, compared with the actual measurement. Except for sand wave No.5, its height is only one-third of the actual wave height. It is also shown that the location of the sand wave peaks and troughs are comparable to the measurement data but, similar to the pre-dredging case, the shape of the sand waves is not accurately simulated.

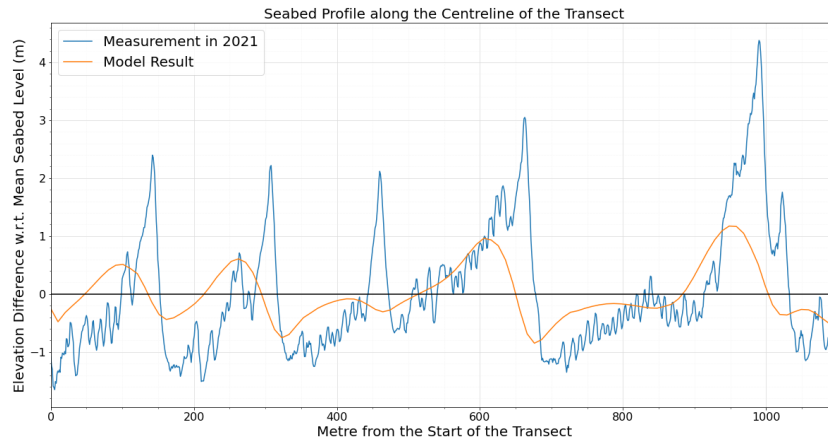


Figure 5.8: Comparison on the Seabed Profile between the Measurement and the Model Result

In addition to the seabed profile, a sediment budget is considered an additional performance indicator. The difference in the sediment budget in different zones between 2016 and 2021 based on the measurement data and the model result is tabulated in Table 5.2. It is shown that a significant sediment loss in the system was encountered in the model and the order of magnitude in the total amount of sediment in the system in the model is way beyond the benchmark. A possible reason is that the actual dredged volume was smaller than the assumption in the model. Nevertheless, the erosion-accretion plot in Figure 5.9c and sediment budget between post-dredging and 2021 in Table 5.3 demonstrate sand wave recovery in the model. In addition, in terms of the sediment budget in the dredged and the non-dredged areas, it is shown that both sides of the trench have the same sediment amount in equivalent metres in both the measurement data and the simulation. This shows that both sides of the trench have the same contribution to the sand wave recovery and the model is capable of simulating the interaction between the dredged and the non-dredged areas.

Location	Benchmark (2016-21)	Simulation Results (2016-21)
Upper Zone	-21,700 (-0.27)	-77,000 (-0.96)
Mid Zone	-16,300 (-0.62)	-62,000 (-2.32)
Lower Zone	-16,800 (-0.23)	-72,000 (-0.97)
Total	-54,800	-211,000

Table 5.2: Sediment Budget of the Benchmark and the Simulation in m^3 (values in brackets represent the sediment budget in equivalent metre)

Location	2016 - Pre-dredging (2018)	Pre- and Post-dredging	Post-dredging (2018) - 2021
Upper Zone	-6.17 (-0.00)	-68,000 (-0.85)	-9,200 (-0.11)
Mid Zone	-210 (-0.01)	-81,000 (-3.06)	19,900 (0.75)
Lower Zone	720 (0.01)	-63,000 (-0.85)	-9,900 (-0.13)
Total	-500	-212,000	800

Table 5.3: Breakdown of the Sediment Budget (m^3) in Different Periods in the Model
(values in brackets represent the sediment budget in equivalent metre)

5.5. Discussion of the Results

5.5.1. Hydrodynamic and Morphodynamic Perspective of sand wave recovery

To understand the hydrodynamics and morphodynamics of sand wave recovery, the direction of the depth-averaged flow vector and bed-load transport vector are considered. Figure 5.10a shows the direction of the depth-averaged flow vector in blue and bed-load transport vector in red approximately 70m away from the Northern side of the trench, whereas Figure 5.10b shows the direction of the same vectors at the Northern edge of the trench. It is shown that as the location is closer to the trench, the angle of bed-load transports deviates from the direction of the flow. This is due to the effect of the transverse slope effect inducing an additional downslope vector. Thus, the angle of the resultant bed-load transport deviates from the flow direction.

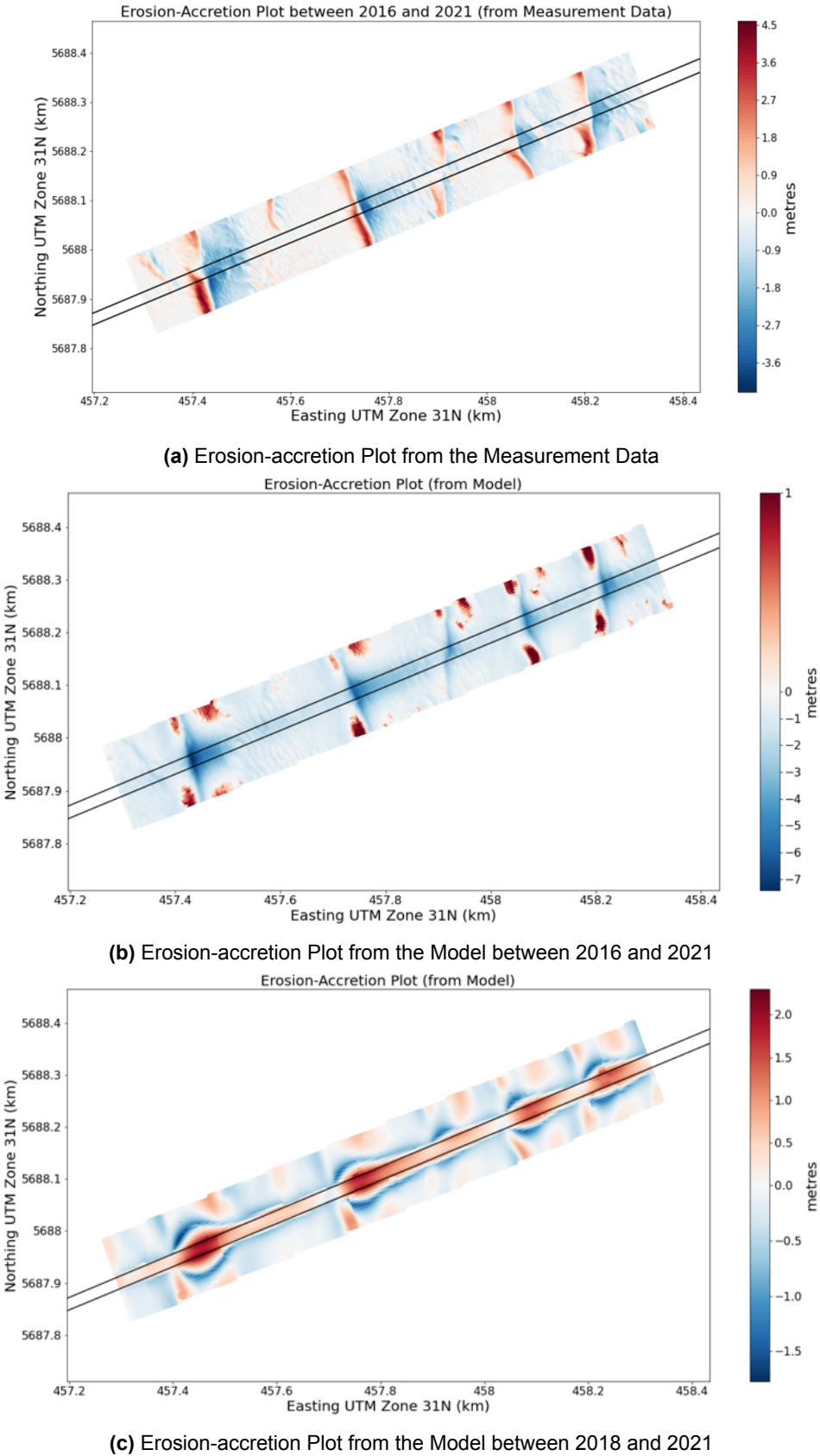


Figure 5.9: Results Comparison between Measurement Data and Model Result

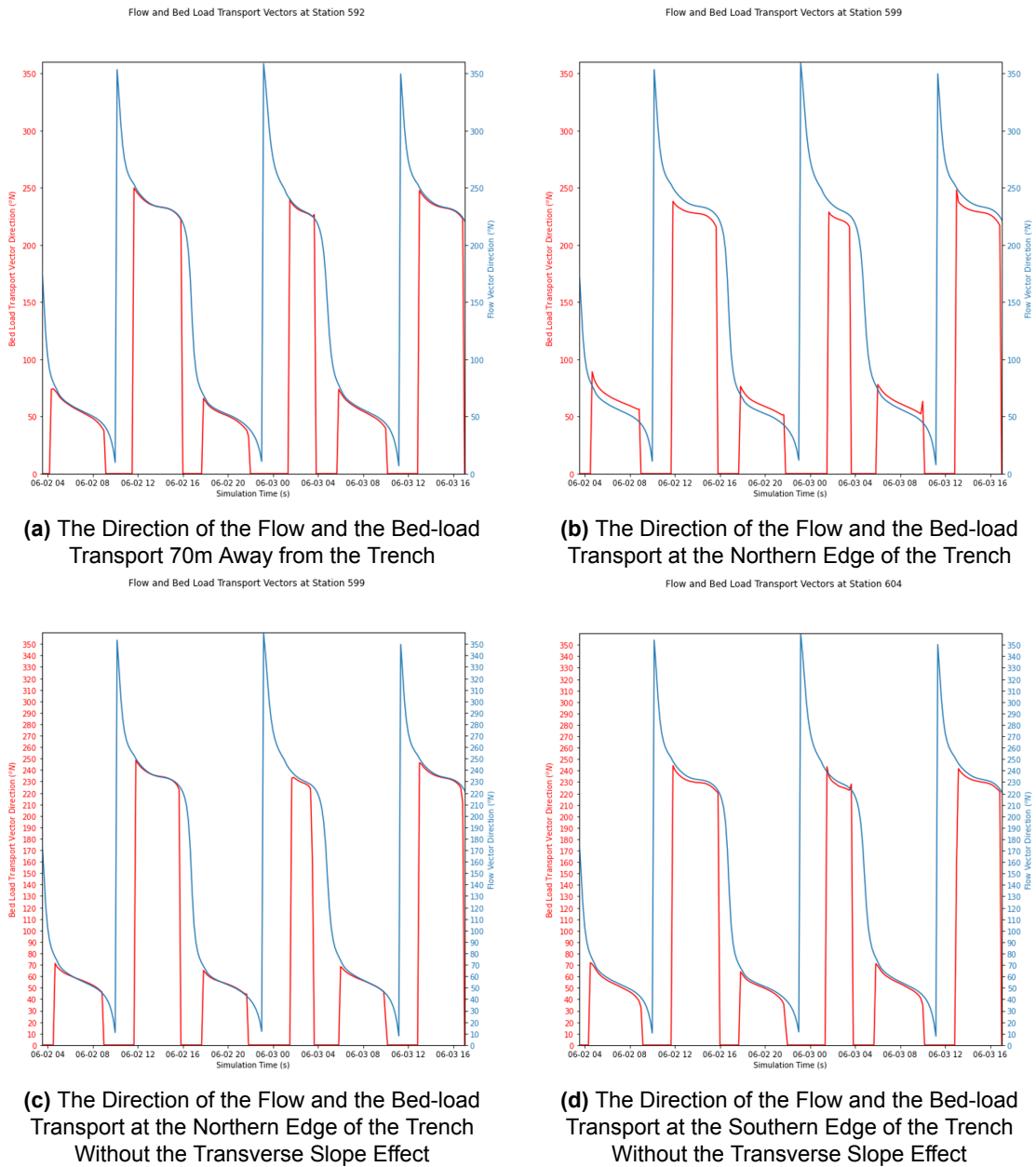


Figure 5.10: The Direction of Flow and the Bed-load Transport at Different Locations With and Without the Transverse Slope Effect

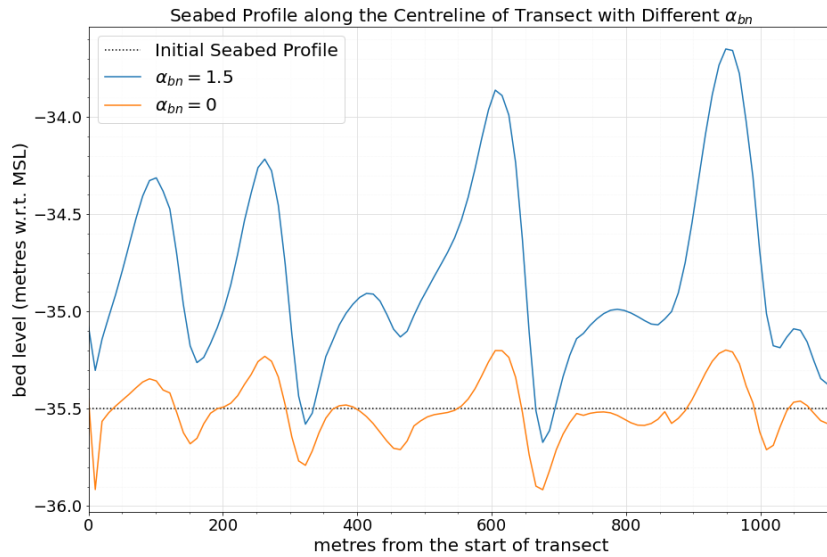


Figure 5.11: Comparison on the Seabed Profile with and without the Transverse Slope Effect between 2018 and 2021

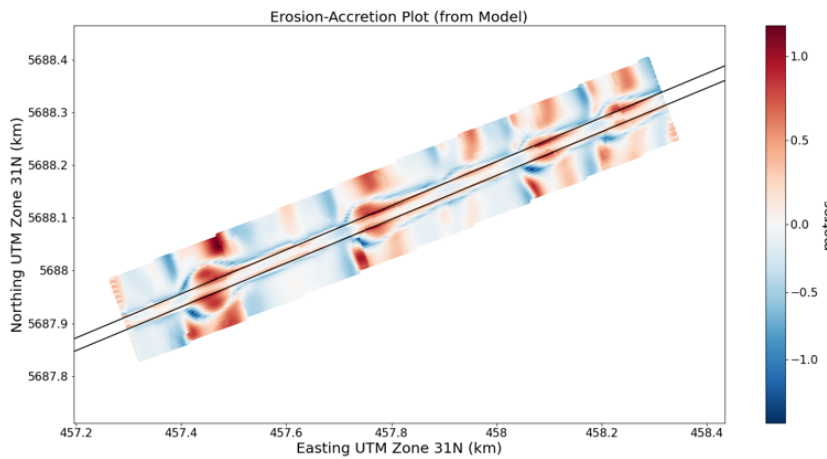


Figure 5.12: Erosion-accretion Plot from the Model without α_{bn} between 2018 and 2021

Location	$\alpha_{bn} = 1.5$	$\alpha_{bn} = 0$
Upper Zone	-9,200 (-0.11)	-1,300 (-0.02)
Mid Zone	19,900 (0.75)	3,500 (0.13)
Lower Zone	-9,900 (-0.13)	-2,300 (-0.03)
Total	800	-100

Table 5.4: Sediment Budget (m^3) due to Different α_{bn} Values (values in brackets represent the sediment budget in equivalent metre)

This is confirmed by another simulation with $\alpha_{bn} = 0$ as shown in Figures 5.10c and 5.10d. It shows that the direction of bed-load transport is now parallel to the direction of flow at the trench. In addition, Table 5.4 shows a significant reduction in the sediment volume trapped in the trench after 39 months without contribution by the transverse slope effect. The volume is approximately one-sixth of the original value. It is shown that the transverse slope effect has a significant contribution to sediment transport along the trench and the infilling ability. In addition, it is noted that the total sediment budget of these two

simulations are comparable. This implies that there is no sediment outside the system contributing to the sand wave recovery and the recovered sand waves are mainly due to the sediments from the two sides.

Nevertheless, there is still a considerable amount of sediment trapped in the trench and sand wave recovery as shown in Figures 5.11 and 5.12. This is caused by direct infilling by the oblique flow direction. As shown in Figures 5.10c and 5.10d, taking the Northern side of the trench as an example, during the flood tide when the direction of flow is between 230 and 250°N, there is an angle difference between 5 to 25° with respect to the alignment of the trench. On the contrary, during the ebb tide, when the flow direction is between 50 and 70°N, there is also an angle difference between 5 to 25° with respect to the alignment of the trench. That implies that during the flood tide, the non-dredged area on the Northern side of the trench feeds sediment into the trench, whereas during the ebb tide, the non-dredged area on the Southern side of the trench feeds sediment into the trench.

To summarise, the infilling process of sediment in this case study includes two effects: the sediment transport due to the transverse slope effect and the direct sediment transport by the flow.

5.5.2. Staging in Sand Wave Recovery

Figure 5.13 shows the evolution of the seabed level after different tidal cycles with MORFAC of 30. It is noted that the evolution of the seabed along the transect is similar in other simulations with different MORFACs but the simulation with MORFAC of 30 is chosen for a better illustration. It is shown that the location of peaks and troughs along the transect in the first half tidal cycle are different from their locations in subsequent tidal cycles. The topography becomes stable after the first cycle and starts growing in its amplitude. A non-physical development in the first 20m of the transect is observed. The development of the topography during the first tidal cycle is unrelated to the MORFACs but the tidal forcing.

In addition to the seabed evolution, Figure 5.14 shows the sand waves regeneration rate in the Mid-zone, which is the dredged area, for $\alpha_{bn} = 1.5$ and $\alpha_{bn} = 0$ respectively over time in the post-dredging case. The regeneration rate is the ratio of the sediment infill to the dredging volume in the model. The figure shows a slight logarithmic growth of the sediment budget in the Mid-zone in both simulations. At the end of the simulations, approximately 25% and 5% of the sand waves were recovered in the simulations with and without the transverse slope effect respectively. The figure re-emphasises the significance of the transverse slope effect. However, the sediment budget does not show any obvious staging during the sand wave recovery.

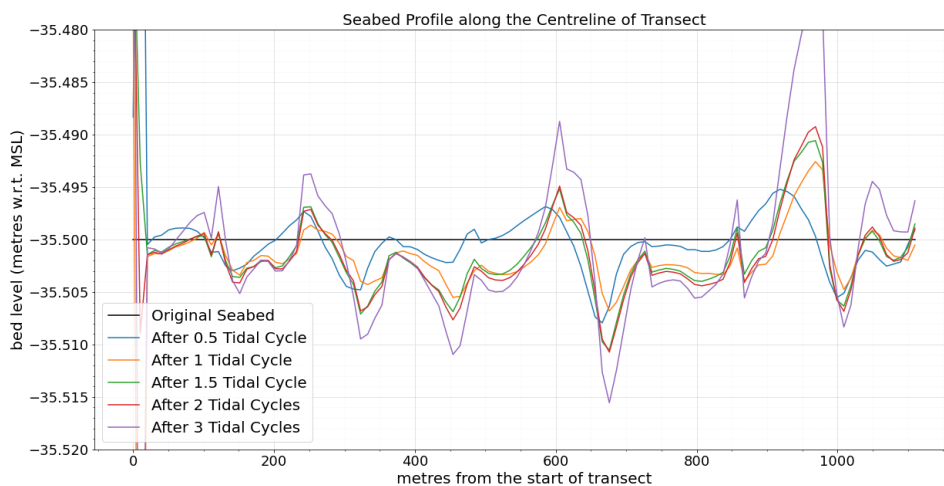


Figure 5.13: Seabed Evolution along the Transect at Different Tidal Cycles (MORFAC = 30)

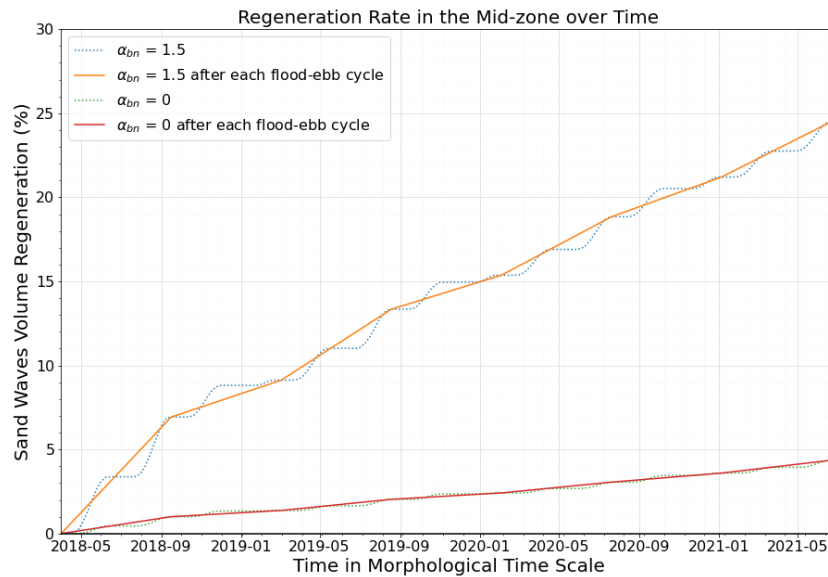


Figure 5.14: Sand Waves Regeneration Rate in the Mid-zone over Time

5.5.3. Outcome of Various MORFAC

Simulations with MORFACs varying from 1 to 360 had been done to give an understanding of the effect of MORFACs on the results. Figure 5.15 shows the seabed level evolution at the original sand wave crest location along the transect. It is shown that the elevation difference among different MORFACs is within 0.2m at any moment. In addition, Figures 5.16 to 5.19 show comparisons of the seabed elevation between different MORFACs under the same morphological time scale. Based on these results, it is shown that simulations with the MORFAC of less than 360 would result in the same shape of topography with a slight difference in the exact topographic level.

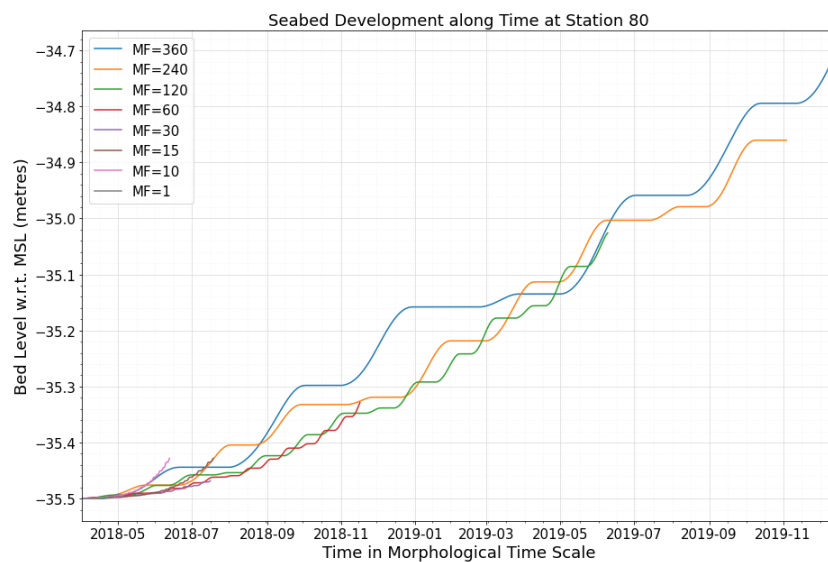


Figure 5.15: Seabed Development at the Sand Wave Crest Location along the Transect

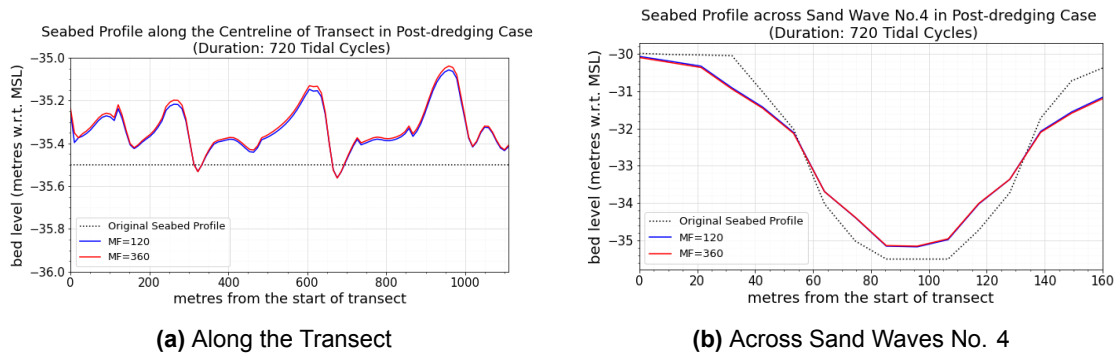


Figure 5.16: Results Comparison between MF = 120 and 360 in the Morphological Time Scale of 720 Tidal Cycles

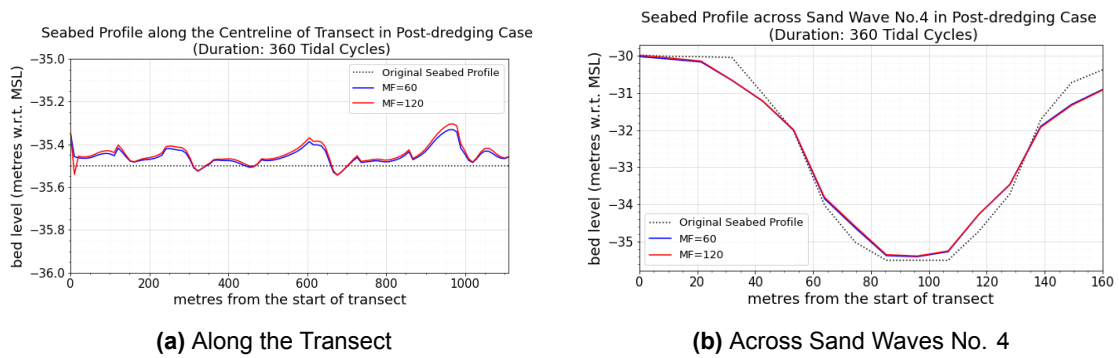


Figure 5.17: Results Comparison between MF = 60 and 120 in the Morphological Time Scale of 360 Tidal Cycles

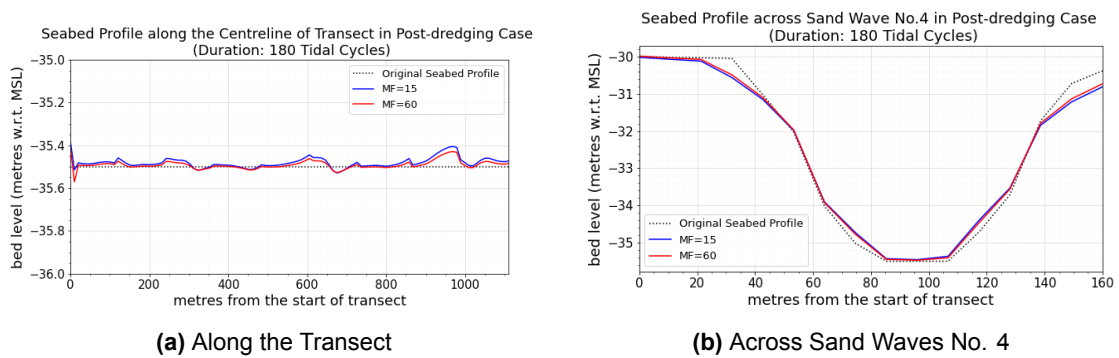


Figure 5.18: Results Comparison between MF = 15 and 60 in the Morphological Time Scale of 180 Tidal Cycles

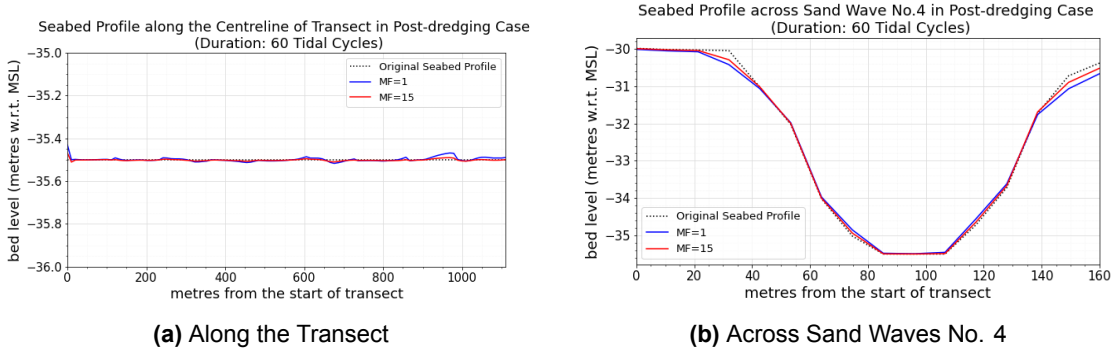


Figure 5.19: Results Comparison between MF = 1 and 15 in the Morphological Time Scale of 60 Tidal Cycles

6

Discussion

Previous chapters describe the methodology and findings from the case study and numerical modelling and this chapter deliberates on the implications and limitations of the thesis.

6.1. Sand Wave Recovery Mechanisms

This numerical model is the first 3D numerical model simulating sand wave recovery and it reveals that the sediment transport due to the transverse slope effect and the direct infilling by an oblique flow supply sediment into the trench, and thus, cause sand wave recovery. The mechanism of the sediment infill is due to the sediment mobilisation by the bed shear stress induced by the flow and enhanced by the gradient of the sides of the trench. The sand wave recovery process after pre-sweeping is not only dependent on the flow, sediment property or morphology but also on the configuration of the trench.

In addition, the numerical modelling shows that sand wave recovery after pre-sweeping is a local redistribution of sediment. The sediment budget shows that the system neither loses nor gains any significant amount of sediment in the model and the sides of the trench equally contribute sediment infill. The equal contribution could be due to the symmetrical cross-section of the trench and the symmetrical property of flood and ebb tides.

On the other hand, this numerical modelling shows the relationship between the amplitude of the recovered sand waves and the amount of sediment infill from the sides. The amplitude of the recovered sand waves is positively proportional to the amount of sediment infilled into the trench. The more sediment infilled into the trench, the higher recovered sand waves are. This is demonstrated by the simulations with and without the transverse slope effect. By excluding the additional sediment transport induced by the transverse slope effect, the amount of sediment infill and the amplitude of the sand waves are reduced at least half as shown in Figure 5.11.

The dominant sediment transport regime in the model is limited to bed-load transport and it is intriguing to know how suspended load transport contributes to sand wave recovery. Assuming that the suspended load transport is not dominant to dampen the growth of sand waves, suspended load transport is possible to supply sediments from two sides to the trench during the slack water of flood and ebb tides. During flood or ebb tides, ocean current stirs up sediment into the water column and the lifted sediment settles into the trench during the slack water. Since the trench is a local depression, it is difficult to bring sediment out from the trench. As a result, suspended load transport provides additional sediment infill and this could possibly expedite the sand wave recovery. Thus, further research in a circumstance where both sediment regimes are dominant is recommended.

6.2. Staging of Sand Wave Recovery

The model results show that sand wave recovery consists of two distinct periods. The first period refers to the instant reaction or adaption of the morphology to the forcing and the second period refers to the

growth of a developed feature. As shown in Figure 5.13, a particular morphological feature is developed during the first tidal cycle and then this morphological feature becomes stable and starts growing in its amplitude in the following period. This thesis reveals the morphological development in relation to the forcing.

Nevertheless, such staging is not apparent in the regeneration rate over time as shown in Figure 5.14 but the model result shows the logarithmic growth of the sand waves, which is similar to the regeneration period in the Race Bank Offshore Windfarm as shown in Figure 3.8. A possible reason is that the dredged profile in the model was assumed perfectly horizontal, while the dredged profile in reality must contain irregularity and variation due to the dredging work. The instantaneous adaption of such irregularity and variation to the forcing is perhaps missing in the model. It is believed that a numerical simulation with a real dredged profile could provide benefits in terms of the application and more understanding of its instantaneous behaviour after dredging.

6.3. Capability of Delft3D FM in Modelling Sand Wave Recovery

This thesis demonstrates the capability of Delft3D FM on simulating sand wave recovery process. The profile along the transect and the sediment budget show sand waves recovered after the simulation. As shown in Figure 5.8, the location of the peaks and troughs of the recovered sand waves are comparable to the actual measurement data. In the meantime, from the sediment budget as shown in Table 5.2, it is shown that both sides of the trench equally contribute to the sediment infill which is successfully captured by the Delft3D FM.

Nevertheless, in accordance with the comparison between the model and the measurement data, it is shown that the amplitude of the recovered sand wave in the model is lower than the observation from the measurement data. This can be interpreted that the amount of sediment infill in the model is less than the actual circumstance. This could be due to the overestimated dredging volume in the model, missing mechanisms contributing to sediment infilling or inaccurate parameters causing underestimated sediment transport. One of the improvements in the model performance can be through the calibration of the user-defined tuning parameter for the transverse slope effect α_{bn} . As explained in Section 5.5.1, this parameter has a significant impact on the infilling quantity. Nevertheless, the current understanding of this parameter on sand wave recovery is limited. Further research on this parameter could have a significant value in improving sand wave recovery modelling. For example, case studies with different configurations of the trench and an extensive seabed survey could provide how this parameter is affected by the trench configuration and how it changes over time.

On the other hand, this model is consistent with past publications regarding the modelled shape of sand waves, such as the 3D model made by Overes [31]. The shape cannot be maintained and was smoothed under the current setting of Delft3D FM in both pre-dredging and post-dredging simulations. Furthermore, the finest grid size in the numerical model should be able to model the shape of asymmetrical sand waves, as shown in Figure 5.1, in terms of spatial discretisation. This 3D numerical model with such fine grid cells still could not improve the performance of Delft3D FM in modelling the shape of sand waves. It is still unknown about the cause of smoothing behaviour and it can be both physical or numerical reasons. For instance, the numerical scheme of the flow or the sediment transport can be diffusive and cause artificial diffusion leading to smoothing morphological features. It is also intriguing to look at the effect of a user-defined tuning parameter for the longitudinal slope effect (α_{bs}). This parameter leads to a preferred downslope direction of bed-load transport, and therefore, diffuses morphological features. Another possible reason could be a missing mechanism contributing shaping of sand waves or upslope sediment transport. Thus, further research on the smoothing in both numerical and physical perspectives is suggested.

Apart from the capability of Delft3D FM on simulating the recovery process, the ability of Delft3D FM to estimate the timescale of sand wave recovery, including the two stages during recovery, is a concern. The duration of the adaption period is approximately 1 or 3 months based on the measurement in the Race Bank Offshore Windfarm. Nevertheless, the adaption period found in the model depends on the forcing. The adaption period is thus the same as the timescale of the forcing, which is one tidal cycle in the model, which deviates from the actual circumstance. A possible reason is the absence of morphological adaption of irregularity in an actual dredging profile. On the other hand, as shown in

the post-dredging case simulation, the height of the recovered sand waves is only half of the measurement data under the same morphological timescale. Thus, it is still a challenge to use Delft3D FM to accurately estimate the timescale of sand wave recovery.

In short, Delft3D FM is able to simulate the mechanism and the development of sand wave recovery but further research is still necessary to achieve a higher accuracy in estimating the recovered height, sediment budget and recovery duration.

6.4. Upscaling with MORFAC and HPC

In this thesis, simulations with MORFAC varying from 1 to 360 were carried out and it is found that the morphological development in these simulations with different MORFAC are similar with a slight difference in the topography elevation only. Through this thesis, it is realised that MORFAC is still an essential upscaling technique in 3D morphological modelling. In this thesis, a numerical model with more than 68,000 cells in the computational grid and 40 sigma-layers is configured. A 30-day simulation with MORFAC of 1 required a week in real time for computation by DelftBlue but the time required can be reduced to less than a day if the MORFAC is increased to 10. A small MORFAC already has a significant enhancement in the computational effort. Thus, a combination of an HPC cluster and MORFAC can significantly reduce the computation time. With the foreseeable future that the HPC will become more powerful and accessible, this will create more opportunities for sophisticated modelling, such as a higher resolution model or long-term modelling.

6.5. Impact of Storm

This thesis reveals how the tidal forcing supplies sediment into the trench and causes the sand wave recovery. From the application perspective, it is beneficial to understand how other forcings affect sand wave recovery. For example, storm or severe weather conditions could probably affect the sand wave recovery or infilling of the trench. Storm or severe weather induces wind-driven circulation. This circulation could be strong enough to mobilise sediment and bring sediment into the trench causing additional infilling. However, it is expected that storms or severe weather conditions have an insignificant impact on the long-term regeneration process of sand wave recovery because the timescale of storms is not comparable to the regeneration timescale, which is in months and years. On the contrary, attention should be given to the adaption period after dredging. As shown in Figure 5.13, a certain form of morphology is under development in the first tidal cycle. According to the linear stability analysis, a certain form of morphology is determined based on a combination of the vertical Stokes Number and the dimensionless resistance parameter. If there is a storm during this adaption period, another form of morphology due to the temporary storm forcing could possibly be formed. How this particular form of morphology interacts with and develops under persistent tidal forcing at a later stage is also a question. Further research to understand the impact of the storm or adverse weather conditions on the adaption of morphology is recommended.

7

Conclusion

Through this master's thesis, literature related to sand wave recovery is reviewed. It is noted that the current publication related to sand wave recovery is scarce and the current models have their limitations, such as its empirical nature and limited dimension of the models. Given this, a case study and a 3D numerical model by Delft3D FM are constructed in this thesis to strive for providing an understanding of the sand wave recovery mechanisms and investigating whether Delft3D FM has the potential to simulate sand wave recovery. By utilising DelftBlue, which is a supercomputer at Delft University of Technology, and the incorporation of MORFAC, the computational effect of the 3D numerical modelling is significantly reduced and the simulations could be completed within a day. After this thesis, the processes contributing to sand wave recovery are acknowledged and it is realised that Delft3D FM can simulate the sand wave recovery. Finally, to conclude this master's thesis, the solutions to the research questions, the limitations of the thesis and recommendations for future research are presented in this chapter.

7.1. Answers to the Research Questions

1. How does a sand wave recover and what are the key processes behind the sand wave recovery process?

A numerical model simulating the sand wave recovery in a case study was built up and the hydrodynamic and morphodynamic processes in the model were studied. From the numerical model results, it is shown that the bed-load transport due to the transverse slope effect and the direct infilling by the flow are two reasons feeding sediment into the dredged area and leading to sand wave recovery in this case study. In addition, it is found that the sand wave recovery is a local redistribution of sediment. Concerning the development of sand wave recovery, it is shown that there are two phases in the recovery process. The first phase is the adaption period, which refers to the immediate reaction or adaptation of the morphology to the forcing, whereas the second phase refers to the following period in which a particular form of feature is developed and starts growing in its magnitude.

2. To what extent is Delft3D FM able to simulate the key sand wave recovery processes after pre-sweeping in a 3D setting?

The model on Delft3D FM is able to perform sand wave recovery and reproduce sediment infilling. The model also demonstrates a promising location of the recovered sand waves and an equal contribution to the recovery by the sides of the trench, which are consistent with the actual measurement. Although the amplitude of the recovered sand waves and the sediment budget in the model are underestimated, compared with the actual measurement data, the reasons behind such underestimation are clear. Consistent with past publications, the model is unable to simulate the shape of sand waves accurately under the current setting with a fine computational grid and tends to diffuse morphological features. It is demonstrated that fine grid cells in a 3D numerical model could not improve the model performance of modelling the shape of sand waves.

3. To what level can Delft3D FM estimate the timescale of sand waves regeneration?

Based on the model results and the literature, it is found that sand wave recovery involves two stages, which are the adaption period and the regeneration period, but Delft3D FM cannot estimate the timescale of neither these two stages individually nor as a whole under the current configuration. Possible reasons are absence of initial adaption of the irregularity on seabed, which is formed by the dredging work, or uncalibrated parameters in the model leading to underestimated sediment infilling amount.

4. What is the order of magnitude of critical MORFAC in modelling 3D morphodynamics of pre-sweeping?

In this study, a detailed comparison of the topographical level among different MORFACs from 1 to 360 is carried out. The results show that simulations with MORFAC varying from 1 to 360 would perform a similar morphological evolution with a slight difference in the exact seabed level only.

7.2. Limitations of This Thesis

Contribution of Suspended Load Transport

This numerical model is limited to bed-load transport and it is possible that suspended load transport thus could possibly expedite sand wave recovery. Providing that the suspended load transport would not dampen the growth of sand waves, suspended load transport can bring additional sediment infill into the trench. Thus, the height of the recovered sand waves could be higher due to more infill. Further research on the contribution of suspended load transport to sand wave recovery is recommended.

Underestimation in the Results

The recovered seabed profile and the sediment budget as shown in Figure 5.8 and Table 4.8 show a considerable discrepancy in the recovered sand waves height and the sediment budget between the model results and the measurement data. This discrepancy is possibly due to uncalibrated parameters, missing infilling mechanism or overestimated dredging volume. According to the current configuration, there is difficulty in estimating recovery duration by Delft3D FM.

Influence of Storm

The forcings involved in this thesis are limited to tidal forcings only but research on the effect of storms and adverse weather conditions on sand wave recovery is valuable in terms of practical application. Wind-driven current due to storms induces additional sediment mobilisation and possibly supply additional sediment infill. This will result in acceleration in the recovery process or affect the initial bedform during the adaption period.

7.3. Recommendations

More Case Studies

More case studies could help gain more understanding of sand wave recovery in several ways. Case studies with different sedimentology can be studied to understand how the composition of sediments and sediment layers affect sand wave recovery. For example, a different composition of sediment affects the dominance of bed load and suspended load transport. This will provide more information related to the contribution to the sand wave recovery by suspended load transport or different sediment grain sizes. Other than the sedimentology, case studies with substantial post-dredging measurement data can help calibrate the tuning parameter α_{bn} , which is found significant to the sand wave recovery. With substantial post-dredging measurement data, this parameter can be calibrated through a sediment budget comparison between the model and the measurement. Through this exercise, more information related to this parameter can be obtained, such as whether this parameter varies over time and how the configuration of a trench or the geometry of sand waves affects this parameter.

Further Research on Storm Effect

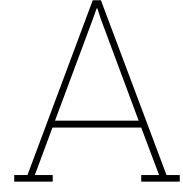
From the application perspective, the duration of the trench remained open, which allows submarine utilities installation work, is concerned. However, a storm or an adverse weather condition during the construction could impact the installation in two ways. It can cause idling of construction and expedite sediment infilling due to wind-driven circulation causing mobilisation of sediment. As a result,

the window for the installation work would be reduced. In addition, it is found that the dredged profile would experience an adaption period first and adapt to the forcing. Understanding of this adaption of the morphology to the storm is limited. Therefore, a study of the impact of storms or severe weather conditions on the sand wave recovery has a significant value.

References

- [1] Ralph Alger Bagnold. *An approach to the sediment transport problem from general physics*. US government printing office, 1966.
- [2] Jingjing Bao et al. "Morphodynamic response of sand waves in the Taiwan Shoal to a passing tropical storm". In: *Marine Geology* 426 (2020), p. 106196.
- [3] Giovanni Besio et al. "Migrating sand waves". In: *Ocean Dynamics* 53.3 (2003), pp. 232–238.
- [4] P Blondeaux. "Sand ripples under sea waves Part 1. Ripple formation". In: *Journal of Fluid Mechanics* 218 (1990), pp. 1–17.
- [5] BW Borsje et al. "The role of suspended load transport in the occurrence of tidal sand waves". In: *Journal of Geophysical Research: Earth Surface* 119.4 (2014), pp. 701–716.
- [6] Gerhardus Hermanus Petrus Campmans. "Modeling storm effects on sand wave dynamics". In: *University of Twente PhD Thesis* (2018).
- [7] GHP Campmans et al. "Modeling tidal sand wave recovery after dredging: effect of different types of dredging strategies". In: *Coastal engineering* 165 (2021), p. 103862.
- [8] Dip Yu Choy. "Numerical modelling of the growth of offshore sand waves: A Delft3D study". In: (2015).
- [9] European Commission. *2050 long-term strategy*. URL: https://climate.ec.europa.eu/eu-action/climate-strategies-targets/2050-long-term-strategy_en (visited on 2023).
- [10] European Commission. *REPowerEU: affordable, secure and sustainable energy for Europe*. URL: https://commission.europa.eu/strategy-and-policy/priorities-2019-2024/european-green-deal/repower-eu-affordable-secure-and-sustainable-energy-europe_en#investing_in_renewables (visited on 2023).
- [11] Johannes Marinus Damen, Theodore Adriënne Godefrieke Petula van Dijk, and Suzanne JMH Hulscher. "Spatially varying environmental properties controlling observed sand wave morphology". In: *Journal of Geophysical Research: Earth Surface* 123.2 (2018), pp. 262–280.
- [12] Deltares. *D-Morphology, 1D/2D/3D, user manual. Delft3D FM suite 2020*. 2021.
- [13] EMODnet. *EMODnet Bathymetry - Which information layers?* URL: <https://www.emodnet-bathymetry.eu/data-products/which-information-layers>. (accessed: 18.05.2023).
- [14] EMODnet. *EMODnet, Human Activities, Energy, Wind Farms*. 2023-06-05. URL: <https://ows.emodnet-humanactivities.eu/geonetwork/srv/eng/catalog.search#/metadata/8201070b-4b0b-4d54-8910-abcea5dce57f> (visited on 06/26/2023).
- [15] Wind Europe. *Offshore Wind in Europe Key trends and statistics 2019*. 2019.
- [16] Jorgen Fredsoe and Rolf Deigaard. *Mechanics of coastal sediment transport*. Vol. 3. World scientific publishing company, 1992.
- [17] SJMH Hulscher, Michiel AF KNAAPEN, and Olaf Scholl. "Regeneration of dredged sand waves". In: *Marine Sandwave Dynamics, International Workshop, Université de Lille*. Vol. 1. 2000, pp. 93–95.
- [18] Suzanne JMH Hulscher. "Tidal-induced large-scale regular bed form patterns in a three-dimensional shallow water model". In: *Journal of geophysical research: Oceans* 101.C9 (1996), pp. 20727–20744.
- [19] Syunsuke Ikeda. "Lateral bed load transport on side slopes". In: *Journal of the Hydraulics Division* 108.11 (1982), pp. 1369–1373.
- [20] Kazumasa Katoh et al. "The development of sand waves and the maintenance of navigation channels in the Bisanseto Sea". In: *Coastal engineering 1998*. 1999, pp. 3490–3502.

- [21] MAF Knaapen. "Sandwave migration predictor based on shape information". In: *Journal of Geophysical Research: Earth Surface* 110.F4 (2005).
- [22] Janneke Krabbendam et al. "Modelling the past and future evolution of tidal sand waves". In: *Journal of marine science and engineering* 9.10 (2021), p. 1071.
- [23] Janneke M Krabbendam et al. "Do tidal sand waves always regenerate after dredging?" In: *Marine Geology* 451 (2022), p. 106866.
- [24] SIGNE MIE LARSEN, ANDREAS ROULUND, and DUNCAN LEE MCINTYRE. "REGENERATION OF PARTIALLY DREDGED SANDWAVES". In: *Coastal Sediments 2019: Proceedings of the 9th International Conference*. World Scientific. 2020, pp. 3026–3039.
- [25] SM Larsen et al. "Sandwaves and megaripples at Race Bank (UK) offshore windfarm". In: *Scour and Erosion: Proceedings of the 8th International Conference on Scour and Erosion (Oxford, UK, 12-15 September 2016)*. CRC Press. 2016, p. 237.
- [26] Nemo Link. "Environmental Statement Volume I". In: *Environmental Statement* (2013).
- [27] IN McCave. "Sand waves in the North Sea off the coast of Holland". In: *Marine geology* 10.3 (1971), pp. 199–225.
- [28] Robin Morelissen et al. "Mathematical modelling of sand wave migration and the interaction with pipelines". In: *Coastal Engineering* 48.3 (2003), pp. 197–209.
- [29] Attila A Németh, Suzanne JMH Hulscher, and Huib J de Vriend. "Modelling sand wave migration in shallow shelf seas". In: *Continental Shelf Research* 22.18-19 (2002), pp. 2795–2806.
- [30] Ørsted. "Appendix 11 to Deadline I submission - Sandwave Clearance Clarification Note". In: *Hornsea Project Three Offshore Wind Farm* (2018).
- [31] Pauline Overes. "Modeling Sand Wave Field Dynamics in the North Sea using Delft3D Flexible Mesh". In: (2021).
- [32] Pauline Helena Petronella Overes. "Efficient modelling of sand wave field dynamics for offshore engineering activities.: Literature report". In: (2022).
- [33] Roshanka Ranasinghe et al. "Morphodynamic upscaling with the MORFAC approach: Dependencies and sensitivities". In: *Coastal engineering* 58.8 (2011), pp. 806–811.
- [34] Graeme M Smart. "Sediment transport formula for steep channels". In: *Journal of Hydraulic Engineering* 110.3 (1984), pp. 267–276.
- [35] N Terseleer et al. "Dynamics of very-large dunes in sandbank areas subjected to marine aggregate extraction, Belgian continental shelf". In: *Van Landeghem, KJJ, Garlan T., Baas, JH* 216 (2016).
- [36] PK Tonnon, LC Van Rijn, and DJR Walstra. "The morphodynamic modelling of tidal sand waves on the shoreface". In: *Coastal Engineering* 54.4 (2007), pp. 279–296.
- [37] W Van Gerwen et al. "Modelling the effect of suspended load transport and tidal asymmetry on the equilibrium tidal sand wave height". In: *Coastal Engineering* 136 (2018), pp. 56–64.
- [38] Leo C Van Rijn. *Principles of sediment transport in rivers, estuaries and coastal seas*. 1993.
- [39] Joh Van Veen. "Sand waves in the North Sea". In: *The International Hydrographic Review* (1935).
- [40] Els Verfaillie, Vera Van Lancker, and Marc Van Meirvenne. "Multivariate geostatistics for the predictive modelling of the surficial sand distribution in shelf seas". In: *Continental Shelf Research* 26.19 (2006), pp. 2454–2468.
- [41] Firmij Zijl, Jelmer Veenstra, and Julien Groenenboom. *The 3D Dutch Continental Shelf Model-Flexible Mesh (3D DCSM-FM) Setup and Validation*. 2018.



Sensitivity Analysis of Various Parameters

A.1. Use of Different Van Rijn Formulations

A.1.1. Van Rijn (1993 & 2007) Formulations

Van Rijn (1993) Formulation has the following expression for bed-load transport:

$$S_b = 0.006\rho_s w_s d_{50} M^{0.5} M_e^{0.7} \quad (\text{A.1})$$

where ρ_s is the density of sediment, w_s is the settling velocity, d_{50} is the median grain size, M is the sediment mobility number and M_e is the excess sediment mobility number.

The sediment mobility number and the excess sediment mobility number are expressed as follows:

$$M = \frac{u_r^2}{\left(\frac{\rho_s}{\rho_w} - 1\right)gd} \quad (\text{A.2})$$

$$M_e = \frac{(u_r - u_c r)^2}{\left(\frac{\rho_s}{\rho_w} - 1\right)gd} \quad (\text{A.3})$$

where u_r is the velocity of flow, ρ_w is the density of water, g is the gravitational acceleration and d is the diameter of sediment.

Van Rijn (2007) Formulation has the following expression for bed-load transport:

$$S_b = \gamma \rho_s \rho_{50} D_*^{-0.3} \left(\frac{\tau'_{b,c}}{\rho_w}\right)^{0.5} \left(\frac{\tau'_{b,c} - \tau_{b,cr}}{\tau_{b,cr}}\right) \eta \quad (\text{A.4})$$

where γ is a constant of 0.5, ρ_s is the density of sediment, d_{50} is the median grain size, D_* is the dimensionless particle diameter, ρ_w is the density of water, $\tau'_{b,c}$ is the grain-related bed-shear stress due to currents and $\tau_{b,cr}$ is the critical bed shear stress.

A.1.2. Results Comparison

Figures A.1 and A.2 show the results in the simulations of pre-dredging and post-dredging cases respectively with different van Rijn formulation. It is shown that van Rijn (1993) formulation provides a less diffusive result, compared with van Rijn (2007) formulation.

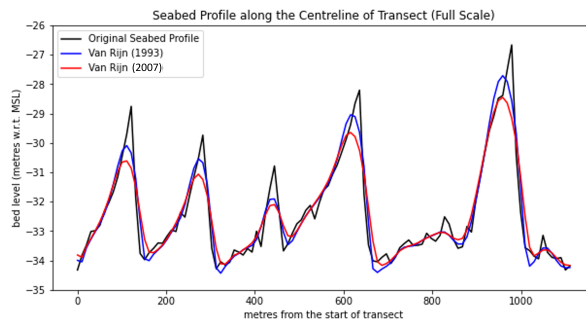


Figure A.1: Simulation Results along the Trench in the Pre-dredging Case

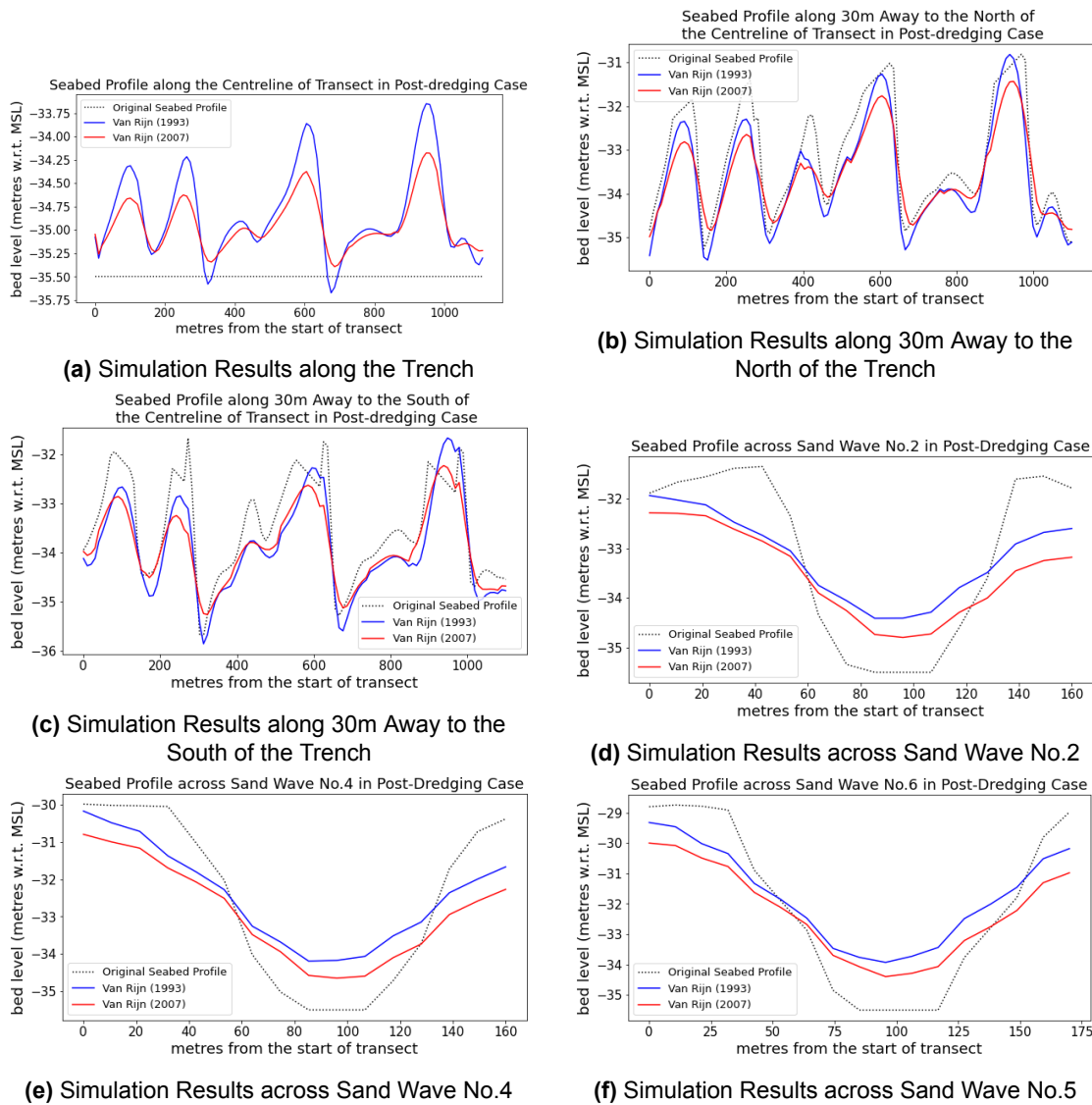


Figure A.2: Difference between Van Rijn (1993 & 2007) Formulation in the Post-dredging Case

A.2. User-defined Tuning Parameter (α_{bs})

Two different values in α_{bs} , 1.5 and 3.0, were tested in both pre-dredging and post-dredging cases and the results are shown in Figure A.3 and Figures A.4 respectively. Simulations in both cases show that the results are less diffusive when α_{bs} is equal to 1.5. Thus, 1.5 in α_{bs} was adopted.

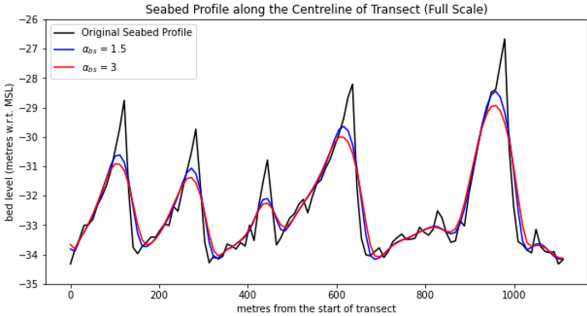


Figure A.3: Simulation Results along the Trench in the Pre-dredging Case

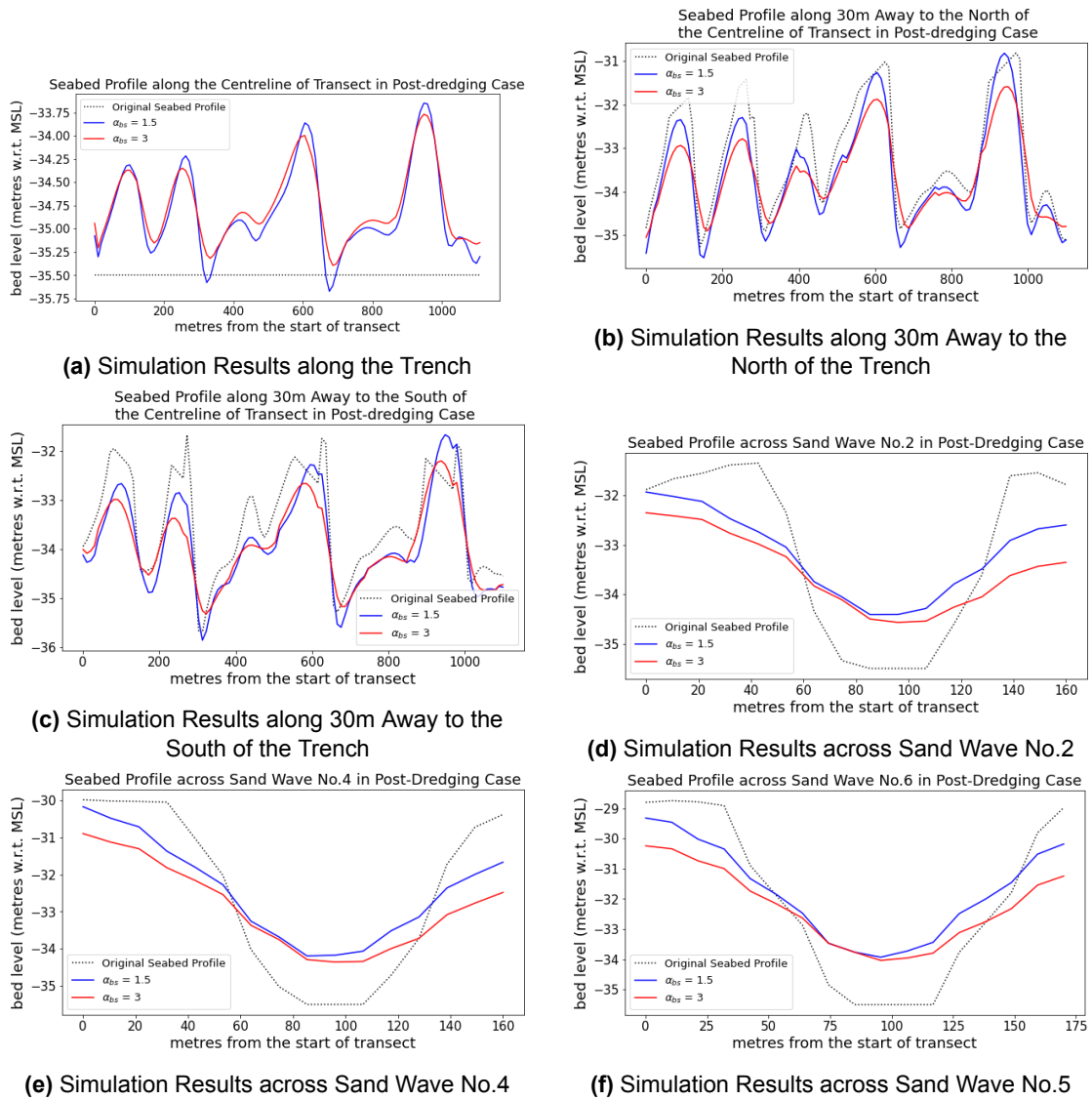


Figure A.4: Difference between Different Value of α_{bs} in the Post-dredging Case

A.3. Median Grain Size

Two different sizes of the median grain size, $350 \mu m$ and $400 \mu m$, were tested to see how the median grain size affects the results in both pre-dredging and post-dredging cases. Figures A.5 and A.6 show the results with different median grain sizes in pre-dredging case and post-dredging case respectively. As shown, no difference between different median grain sizes were observed in the pre-dredging case, whereas there is an insignificant difference at recovered sand waves peak in the post-dredging case.

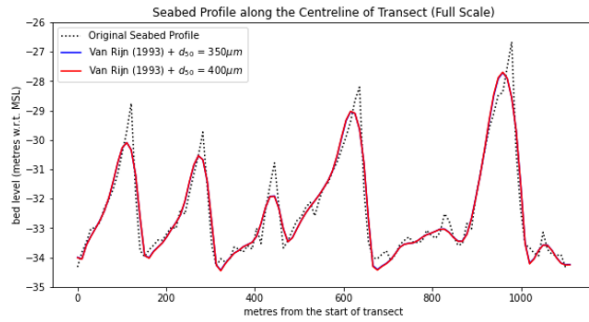


Figure A.5: Simulation Results along the Trench in the Pre-dredging Case

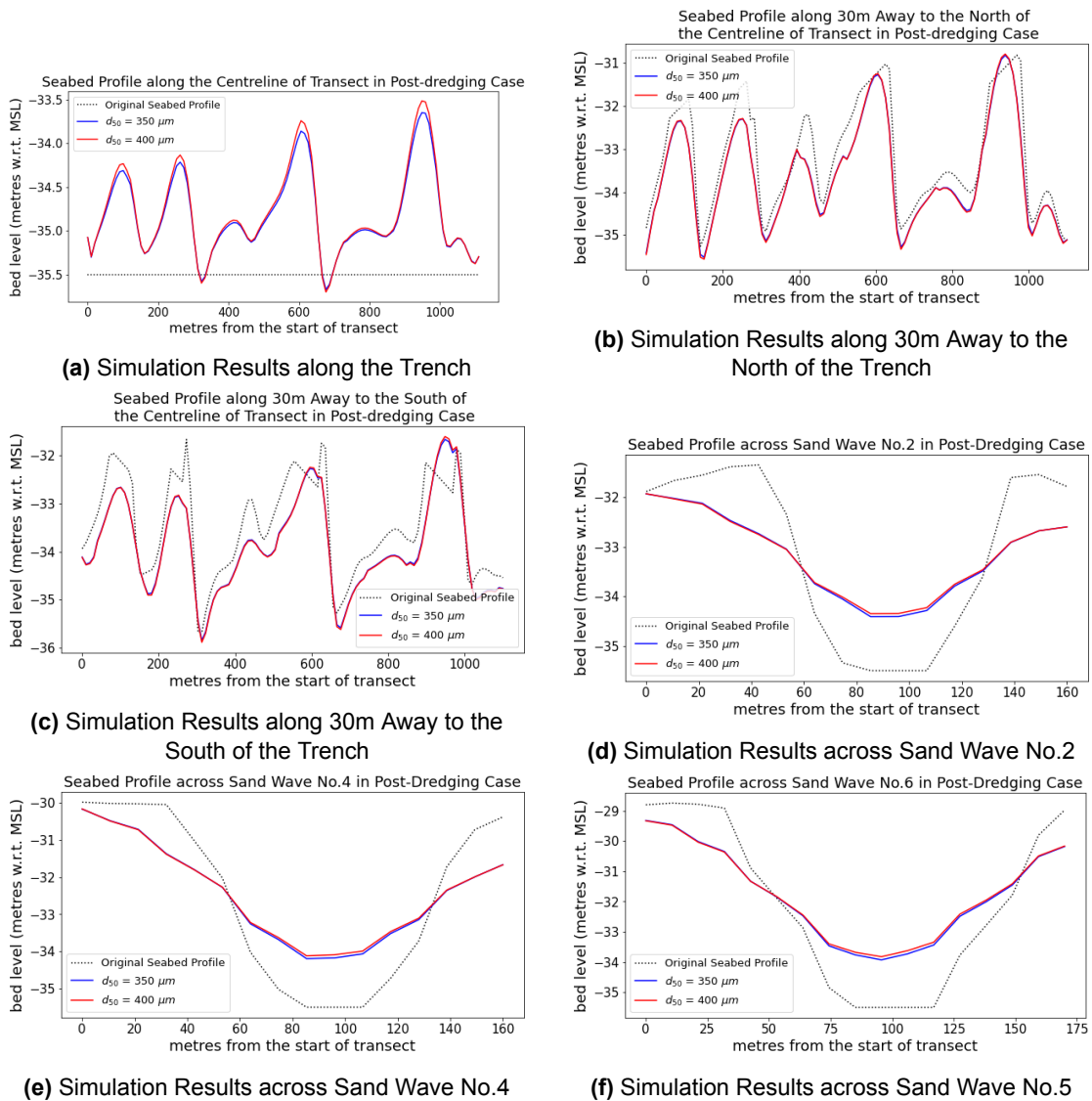


Figure A.6: Difference between Different Median Grain Size in the Post-dredging Case